Below-canopy contributions to ecosystem CO2 fluxes in a temperate mixed forest in Switzerland

Journal Article

Author(s):
Paul-Limoges, Eugénie; Wolf, Sebastian (iD); Eugster, Werner (iD); Hörtnagl, Lukas (iD); Buchmann, Nina (iD)

1 **Below-canopy contributions to ecosystem CO$_2$ fluxes in a temperate mixed forest in**

2 **Switzerland**

3

4 E. Paul-Limoges[*1], S. Wolf[2], W. Eugster[1], L. Hörtnagl[1], N. Buchmann[1]

5 [1]Institute of Agricultural Sciences, ETH Zurich, Universitätsstrasse 2, 8092 Zurich, Switzerland

6 [2]Institute of Terrestrial Ecosystems, ETH Zurich, Universitätsstrasse 22, 8092 Zurich, Switzerland

7

8 [*] Corresponding author. E-mail address: eugenie.paul@usys.ethz.ch

9

12

13 **Abstract**

14 Forests are structurally complex ecosystems with several canopy layers, each with

15 distinct functional properties contributing differently to the net ecosystem CO$_2$ exchange. A large

16 number of studies have addressed ecosystem-scale net CO$_2$ fluxes in forests, but only few studies

17 have investigated the role of the forest understory. The goal of this study was to quantify the

18 below-canopy contribution to ecosystem CO$_2$ fluxes of a mixed deciduous forest in Switzerland.

19 Below and above-canopy eddy-covariance (EC) measurements were made continuously over two

20 years, complemented by within canopy wind and CO$_2$ concentration profile measurements.

21 On an annual basis, the below-canopy fluxes indicated a net carbon source dominated by

22 soil respiration, while the above-canopy fluxes were dominated by tree photosynthesis leading to

23 a net carbon sink. Below-canopy fluxes showed a net carbon sink only in spring, with the early

24 emergence of understory plants before overstory canopy leaf-out. Below-canopy respiration

25 partitioned from the EC measurements agreed well with previous chamber-based soil respiration

26 measurements. However, below and above-canopy fluxes became decoupled under full canopy

27 closure, thus leading to unaccounted below-canopy fluxes when measured only above the

28 canopy. Wind and CO_2 concentration profile measurements supported this finding. Decoupling

29 was independent of low turbulence conditions and decoupled periods could be identified using

30 the relationship between the below and above-canopy standard deviation in vertical wind

31 velocity. A decoupling correction was applied to the above-canopy measurements during

32 decoupled periods and corrected annual net ecosystem production (NEP) agreed well with

33 independent estimates from biomass inventory combined with models. Overall, the below-

34 canopy fluxes contributed 79% to annual ecosystem respiration, but only 9% to annual

35 ecosystem photosynthesis. The decoupling correction reduced annual NEP for the site from

36 about 760 to 330 g C m^{-2} yr^{-1}. Our results showed that below-canopy EC measurements are

37 essential in this mixed deciduous forest, and likely in many other forests, to fully understand the

38 carbon dynamics within structurally complex ecosystems.

39

40 **1. Introduction**

41 Forests play an important role in the global carbon cycle by sequestering up to 30% of

42 anthropogenic CO_2 emissions (Pan et al., 2011). The magnitude of CO_2 sequestered by a forest

43 varies depending on many factors such as climate, species composition, growth strategy

44 (deciduous or evergreen), stand age and structure (Luyssaert et al., 2007). Forests are structurally

45 complex ecosystems, both vertically and horizontally. In many cases, several layers with distinct

46 functional properties contribute differently to the CO_2 exchange, both in the understory and the

47 overstory (Misson et al., 2007). Although a large number of studies have addressed ecosystem-

48 scale net CO_2 fluxes in forests, only a limited number of studies have investigated the below-

49   canopy contribution, i.e. from understory vegetation and soil, to these ecosystem fluxes

50   (Baldocchi and Vogel, 1996; Baldocchi et al., 1997; Black et al., 1996; Constantin et al., 1999;

51   Falk et al., 2008; Launiainen et al., 2005; Law et al., 2001; Misson et al., 2007).

52   The net CO_2 exchange between a forest and the atmosphere is commonly measured above

53   the canopy using the eddy-covariance (EC) technique (Baldocchi, 2003). Net ecosystem

54   production (NEP) depends on the balance between the amount of CO_2 fixed by gross primary

55   production (GPP) and the amount released through ecosystem respiration (R) (i.e., NEP = GPP −

56   R). EC measurements of CO_2 fluxes at different heights in forests can be used to separate the flux

57   contribution from below the main canopy to the total ecosystem flux (Misson et al., 2007).

58   Although in some instances such measurements can be problematic due to low wind speed and

59   intermittent turbulence, some studies have shown that subcanopy CO_2 fluxes can be successfully

60   measured after screening out problematic measurements (Baldocchi and Vogel, 1996; Baldocchi

61   et al., 1997; Black et al., 1996; Constantin et al., 1999; Falk et al., 2008; Launiainen et al., 2005;

62   Law et al., 2001; Misson et al., 2007).

63   From the limited number of studies that have thus far investigated the contribution of

64   below-canopy to ecosystem CO_2 fluxes, large variations in below-canopy contributions have

65   been found among sites. While some studies reported that the understory vegetation and soil

66   provided no contribution to stand level NEP fluxes (Rannik et al., 2002), others have shown that

67   even a slight surface moss layer can offset soil respiration losses during days with high

68   irradiance (Janssens et al., 2001). Depending on the leaf area index (LAI) of the overstory, more

69   or less light penetrates through the canopy to the understory vegetation and soil. Most understory

70   species have thus adapted to the low light levels, either by achieving their maximum LAI before

71   canopy leaf emergence, the "phenological escape" (Crawley, 2009; Richardson and O'Keefe,

3

72   2009), or by reaching a higher quantum yield efficiency at lower irradiance levels (Jones, 2014;

73   Larcher, 2003). The contribution from below-canopy photosynthesis and respiration will

74   therefore depend largely on the specific ecosystem. Understory photosynthesis has been found to

75   contribute between 0 and 39% to total canopy GPP (Misson et al., 2007; Siqueira et al., 2006),

76   while below-canopy respiration represents a larger proportion of the respective total ecosystem

77   respiration flux at 32 to 79% (Law et al., 1999; Misson et al., 2007). The understory vegetation

78   and soil in deciduous broadleaf forests typically contributes more to ecosystem respiration (62%)

79   compared to evergreen coniferous forests (49%) (Misson et al., 2007), often due to differences in

80   understory biomass and/or to the greater amount of nutrients, especially nitrogen, in the

81   decomposing leaves compared to needles (Reich et al., 2003). As the below-canopy contribution

82   depends greatly on specific ecosystems, extrapolation across sites is difficult.

83   Below-canopy EC measurements also have the potential to provide insights on errors in

84   above-canopy EC measurements, particularly due to low turbulence conditions below the forest

85   canopy layer. In some instances, this can help understanding the advection problem, which is

86   present to varying extents at most EC sites. As several studies have indicated thus far, advection

87   is difficult to quantify, even with extensive advection measurement campaigns (Aubinet et al.,

88   2010). A study by Etzold et al. (2010) estimated the influence of advection on the CO_2 flux

89   measured at the Lägeren site in Switzerland during one growing season. Advection accounted for

90   36% of NEP and, as in most other advection studies, filtering low turbulence periods with a u_*-

91   threshold was suggested to compensate for the advective losses of CO_2. Several studies have

92   found additional insights linked to advection for specific sites using below-canopy EC

93   measurements (Burns et al., 2011; Cook et al., 2004; Foken et al., 2012; Jocher et al., 2017;

94   Novick et al., 2014; Staebler and Fitzjarrald, 2004; Thomas et al., 2013; Tota et al., 2008;

95 Vickers et al., 2012; Vickers and Thomas, 2013). Tota et al. (2008) found a significant below-

96 canopy transport of respired CO_2 in an Amazonian tropical rainforest, which was missed when

97 relying only on above-canopy EC measurements, and thus the very large uptake previously

98 reported for the site was incorrect. Jocher et al. (2017) found that the apparent CO_2 uptake

99 measured in winter at a boreal site in northern Sweden was due to the effect of local topography,

100 resulting in a decoupling of the below-canopy air mass from the above-canopy air mass. Thomas

101 et al. (2013) used below-canopy EC measurements to improve the above-canopy NEP estimate

102 of a tall and dense Douglas-fir forest in Oregon, where decoupling below the canopy also led to

103 unrealistically high NEP above the canopy.

104   The overarching goal of this study was to improve the understanding of ecosystem-level

105 CO_2 exchange in a temperate mixed forest in Switzerland using below and above-canopy EC

106 measurements over two years. The specific objectives of this study were to 1) quantify the below

107 and above-canopy CO_2 fluxes, both in terms of photosynthesis and respiration, 2) identify

108 decoupling using the below-canopy fluxes and correct the above-canopy fluxes accordingly, 3)

109 quantify the below-canopy contribution to ecosystem CO_2 exchange, and 4) investigate

110 differences between below-canopy and ecosystem functional responses to environmental drivers.

111

112 **2.   Methods**

113 **2.1   Research site**

114   The Lägeren forest site (47°28'42" N, 8°21'52" E, 682 m.a.s.l.) is located on the relatively

115 steep (average 24°) south-facing slope of the Lägeren mountain, northwest of the city of Zurich

116 in Switzerland. The Lägeren temperate mixed forest is characterized by a relatively high species

117 diversity and a complex canopy structure, with European beech (*Fagus sylvatica* L.), ash

118   (*Fraxinus excelsior* L.), European silver fir (*Abies alba* Mill.), sycamore maple (*Acer*

119   *pseudoplatanus* L.), and Norway spruce (*Picea abies* (L.) Karst.) as the dominant species. The

120   mean tree height of dominant trees is 30.6 m (Etzold et al., 2011). The understory vegetation is

121   dominated by wild garlic (*Allium ursinum* L.) of a maximum height of 0.4 m during spring and

122   early summer. The separation between the top of the understory vegetation and the bottom of the

123   overstory canopy is about 15 m. The main soil type is a haplic cambisol, and the forest floor litter

124   layer stays rather thin, as most of it decomposes within a year. The site is part of the Swiss Air

125   Quality Monitoring Network (NABEL) since 1986 and of the Swiss FluxNet since 2004

126   (www.swissfluxnet.ch). Mean annual temperature is 7.4 °C, and mean annual precipitation is

127   1000 mm (Etzold et al., 2011).

128

129   **2.2   Profile measurements**

130   CO_2 and H_2O concentrations were measured using an eight-level profile sampling system,

131   with inlet funnels at 0.1, 1, 3, 5, 9, 27, 44 and 54 m above the ground (Etzold et al., 2010). Intake

132   hoses were connected to a home-built valve switching unit with continuously purged air inlets,

133   consisting of an inner ethylene copolymer coating, an aluminum layer and an outer high-density

134   polyethylene jacket (SynflexTM Type 1300, Johannsen AG, Zurich, Switzerland). Airflow was

135   directed through a small pump inside the valve switching unit to a closed-path IRGA (model LI-

136   7000, LI-COR Inc., Lincoln, NE, USA), so that all eight levels were measured by the same

137   IRGA. The flow through the selection unit during measurements was kept at 1 l min^{-1} and at 0.4 l

138   min^{-1} during purging. Switching of the air selection unit and storing of the IRGA analog output

139   (CO_2 concentration, H_2O concentration, cell pressure and temperature) was controlled by a data

140   logger (CR10, Campbell Scientific Inc., Loughborough, UK). Each inlet was consecutively

6

141 selected for 30 s, and the CO_2 concentration for that inlet was measured during the last 10

142 seconds to avoid contamination among the different levels. Each level was measured every 10

143 minutes, and the measurements were then aggregated to 30 min averages. The reference flow

144 path of the IRGA was consistently scrubbed with ascarite and desiccant ($Mg(ClO_4)_2$), and a gas

145 of known CO_2 concentration was used to reference the IRGA measurements every three days.

146 In addition to the CO_2 and H_2O vapor profile, vertical profiles of air temperature and

147 relative humidity (Fischer T/F-Sensors, type 431418, K. Fischer GmbH, Drebach, Germany), as

148 well as wind speed and direction (Gill 2-D sonic anemometers, Gill Instruments Ltd.,

149 Lymington, UK) were measured at six heights (1, 5, 9, 27, 44, and 54 m above the ground).

150 Measurements were controlled and stored by a data logger (CR1000, Campbell Scientific Inc.,

151 Loughborough, UK). The measurement interval was 10 sec, and the measurements were then

152 aggregated to 30 min averages.

153

154 **2.3   Eddy-covariance measurements**

155 Continuous turbulent fluxes of CO_2, water vapor and sensible heat were measured below

156 and above the canopy in 2014 and 2015 using the eddy-covariance (EC) technique (Baldocchi,

157 2003). The below-canopy EC system was at a height of 1.5 m above the soil surface, while the

158 above-canopy EC system was at a height of 54 m. The below-canopy EC system was within the

159 main footprint of the above-canopy EC system. The EC instrumentation at each level consisted

160 of an open-path infrared gas analyzer (IRGA) (model LI-7500, LI-COR Inc., Lincoln, NE, USA)

161 and a three-dimensional ultrasonic anemometer-thermometer (models HS (above) and R3

162 (below), Gill Instruments Ltd., Lymington, UK). EC measurements were made at a frequency of

163 20 Hz. Delays were calculated by maximizing the covariance magnitude at high flux.

164   Half-hourly fluxes of CO_2 (F_c, µmol m^{-2} s^{-1}) were calculated from the covariance of

165   vertical velocity and the CO_2 molar density with WPL correction (Webb et al., 1980). As a

166   previous study by Göckede et al. (2008) showed that a conventional two-dimensional coordinate

167   rotation is better suited at this site than a planar fit approach, the coordinate system was aligned

168   with the mean streamlines so that the mean vertical wind vector became zero (Wilczak et al.,

169   2001). Turbulent departures were then calculated by Reynolds averaging of 30-min blocks of

170   data. A half-hourly averaging period was chosen because it is long enough to capture most of the

171   large eddies (i.e., low frequencies) involved in turbulent transport (Finnigan et al., 2003), and

172   stationarity was generally observed for this duration. Frequency response corrections were

173   applied to raw fluxes, accounting for high-pass (Moncrieff et al., 2005) and low-pass filtering

174   (Horst, 1997) (see Figure S 1 in Supplementary Material for below-canopy cospectra). All fluxes

175   were calculated using the *EddyPro* software (v6.1.0, LI-COR Inc., USA).

176   Net ecosystem exchange (NEE) was calculated as the sum of F_c and the rate of change of

177   CO_2 storage in the air column below the height of the EC flux measurements. The rate of change

178   in CO_2 storage in the air column underneath the above-canopy EC measurement level at 54 m

179   was calculated from the mixing ratio measurements of the LI-7000 IRGA sampling the eight

180   profile levels following Morgenstern et al. (2004). When calculating fluxes for the above EC

181   system in relation to the below-canopy system, the rate of change of CO_2 storage was calculated

182   using the profile measurements between the above and below-canopy EC system. Assuming that

183   fluxes of methane and other volatile organic compounds, and drainage of dissolved organic and

184   inorganic C are negligible, NEP was calculated as – NEE. Negative NEP values indicate a

185   release of CO_2 to the atmosphere, while positive values indicate CO_2 uptake by the vegetation.

186   NEP, GPP and R with above or below subscripts refer to the respective measurement levels.

8

187

2.4 Auxiliary measurements

Above-canopy measurements of climatic variables were made at a height of 54 m. Air temperature (T_a) and relative humidity (RH) were measured using a temperature and relative humidity probe (Rotronic MP101A, Bassersdorf, Switzerland) inside a radiation shield. Total incoming direct and diffuse photosynthetic photon flux density (PPFD) was measured using a sunshine sensor (BF2, Delta-T Devices, Cambridge, UK), while reflected PPFD was measured using a quantum sensor (PARlite, Kipp & Zonen B.V., Delft, The Netherlands). Net radiation (R_n) was measured using a CNR 1 four-way net radiometer (Kipp & Zonen B.V., Delft, The Netherlands). The PPFD sensors and CNR 1 were installed pointing south of the tower.

Below-canopy measurements of climatic variables were made at a height of 2 m. Total incoming PPFD was measured using a quantum sensor (LI190SB-L, LI-COR Inc., Lincoln, NE, USA). Soil temperature (T_s) and water content (Θ) were measured at depths of 5, 10, 20, and 30 cm using Decagon ECH$_2$O EC-20 probes (Pullman, WA, USA). Measurements were controlled and stored by a data logger (CR10X, Campbell Scientific Inc., Loughborough, UK); measurements were made every 30 s and output averaged every 10 min.

203

2.5 Leaf area index and biomass measurements

Overstory leaf area index (LAI) was measured using a LAI-2000 (LI-COR Inc., Lincoln, NE, USA) once a month during the 2015 growing season. The same transect of ten measurements through the forest was repeated consecutively two times to take into account the spatial and temporal variability in canopy cover. The growing season for the deciduous trees at Lägeren is typically from May until October.

9

210   Understory biomass was also measured once a month during part of the 2014 growing

211   season and during the full 2015 growing season. Understory green (living) biomass was

212   determined by harvesting two 0.20 m x 0.50 m (0.1 m^2) ground areas. Plant material was dried

213   for 48 h at 60 °C and weighed. Understory LAI was estimated from the understory biomass

214   measurements based on the relationship for *Allium ursinum* defined in Ernst (1979).

215   NEP from allometric functions (NEP$_{biomass}$) was calculated using biomass inventories

216   from the Lägeren forest following the approach detailed in Etzold et al. (2011). NEP$_{biomass}$ was

217   estimated as the change in stored carbon in the biomass (boles, branches, twigs, foliage,

218   reproductive organs, coarse and fine roots, and understory vegetation) over time, thereby using

219   allometric relationships for both belowground and aboveground biomass. This approach thus

220   included the net gain of carbon by tree growth and understory production minus the loss by

221   autotrophic and heterotrophic respiration. Regional species-specific equations were used to

222   convert diameter at breast height (DBH) to volume of branches and twigs (Kaufmann, 2001).

223   Species-specific conversion factors for wood density were applied to convert total tree volume

224   into biomass (Assmann, 1986). Pools of foliage and reproductive organs were modelled based on

225   DBH-dependent functions and agreed well with measured litter fall. Coarse root biomass of trees

226   was estimated as a function of DBH, while fine root biomass was estimated as 50% of foliage

227   biomass (de Wit et al., 2006). For more details on these calculations see Etzold et al. (2011).

228   Biomass inventories from 2015 were compared to those from 2005 and 2009 to calculate the

229   mean change in biomass for the forest over these years to give an estimate of the NEP$_{biomass}$ for

230   2015.

231

2.6 Flux analysis and gap filling

2.6.1 Quality control

Data quality checks were performed daily to ensure that malfunctioning instruments were repaired quickly, thereby ensuring almost continuous data for below and above-canopy EC measurements in 2014 and 2015. The statistical quality of the raw time series was assessed before flux calculations following Vickers and Mahrt (1997). Raw high-frequency data were rejected if (1) spikes accounted for more than 1% of the time series, (2) more than 10% of available data points were statistically different from the overall trend in the half-hour period, (3) raw data values were outside a plausible range, or (4) window dirtiness of the IRGA sensor exceeded 80%. Only raw data that passed all quality tests were used for flux calculations. Half-hourly averaged flux data were rejected if (1) CO_2 fluxes were outside a physically plausible range (-50 to +50 μmol m^{-2} s^{-1}), (2) the steady state test statistic was outside the range $\pm30\%$, or (3) the integrated turbulence criterion test was outside the $\pm30\%$ range (Foken et al., 2005). Following the quality tests, 66% (2014) and 70% (2015) of measured data remained for the above-canopy CO_2 fluxes, while 72% (2014 and 2015) of the measured data remained for the below-canopy CO_2 fluxes. Although specific footprint models for below-canopy measurements have yet to be developed, ecosystem-scale footprint models are currently the best available tool to estimate below-canopy footprints (personal communication Natascha Kljun). Based on the footprint model from Kljun et al. 2004, the 90% cumulative footprint area for the below-canopy EC system was estimated to 60 m across slope during daytime and to 200 m at night, while for the above-canopy EC system it was estimated to 200 m across slope during daytime and to 700 m across slope during nighttime. The below-canopy flux footprint was always within the footprint of the above-canopy EC system.

255

2.6.2 Partitioning NEP and filling data gaps

Missing values in the measurement time series were gap filled following Barr et al. (2004). NEP was set equal to GPP – R. R was estimated as –NEP when GPP was known to be zero, i.e., at night and during the cold periods (periods when both T_a and T_s at 5 cm depth were below 0 °C). The gaps in the R time series were then filled based on the annual logistic relationship between R and T_s as follows,

$$R = \frac{r_w(t)r_1}{1+\exp\left[r_2(r_3 - T_s)\right]},\tag{1}$$

where r_1 (μmol m^{-2} s^{-1}), r_2 (°C^{-1}) and r_3 (°C) are model fitted empirical constants. GPP was estimated as NEP + R during daytime or as zero during nighttime and during the cold periods. To fill gaps in GPP data due to gaps in daytime NEP data, a rectangular hyperbolic relationship between GPP and downwelling PPFD was fitted to the GPP data using the equation,

$$GPP = \frac{p_w(t)\alpha Q_\downarrow P_x}{\alpha Q_\downarrow + P_x},\tag{2}$$

where α is the initial quantum yield (mol C mol^{-1} photons), $Q_\downarrow$ is the downwelling PPFD (μmol m^{-2} s^{-1}), and P_x is the photosynthetic capacity (μmol m^{-2} s^{-1}). For both equations, parameters were first obtained for the annual relationships. An additional multiplier, estimated within a 96-point (2-day) moving window, in the numerator of each equation (r_w and p_w) was then allowed to vary over time to account for short-term changes in other environmental variables or phenological stage. The time-varying parameters were determined using a 48-hour moving window moving

12

274   through the year in increments of 12 hours. Finally, gaps in NEP were filled using the difference

275   between modeled GPP and R.

276

277   **2.6.3   Decoupling assessment**

278   Different stability and turbulence based indices (e.g. Richardson number, turbulent

279   kinetic energy) were tested to determine decoupled periods. However, such indices were

280   unsuccessful at determining decoupled periods, as decoupling at the Lägeren site also occurred

281   under high turbulence, unstable conditions. The coupling of the two layers was therefore

282   assessed using the standard deviation of the vertical wind velocity (σ_w) (e.g. Acevedo et al.,

283   2009). Recent studies have shown that the relationship between σ_w below and above-canopy can

284   be used to describe the coupling of the two layers, as the relationship between the two σ_w is

285   linear when the layers are coupled (Jocher et al., 2017; Thomas et al., 2013). Decoupling was

286   therefore assessed based on the linearity of σ_w below and above the canopy. Below and above-

287   canopy σ_w were found to be coupled during the leafless period of the deciduous trees, and to be

288   decoupled during the leaf-on period of the deciduous trees. In order to determine the onset and

289   end of the decoupled period, a 5-day moving window was used to determine the change in the

290   linearity of the σ_w relationship. As a result of the 5-day moving window, the dates selected have

291   an uncertainty of ± 2 days due to transition times in the phenology of the site. As the decoupled

292   periods were linked to canopy cover, an independent approach using the phenological camera

293   (Stardot Netcam SC5; for more details see Ahrends et al. (2008) and Wingate et al. (2015)) on

294   top of the EC tower and the LAI measurements was also tested to determine decoupled periods.

295

3.   Results and Discussion

3.1   Environmental conditions and phenological development

The observed years 2014 and 2015 showed distinct differences in environmental conditions. The 2014 growing season (mid-May to beginning of October) was cooler and wetter, with a mean air temperature of 14.0 °C and 152 mm of rain, compared to the 2015 growing season that had a mean air temperature of 15.6 °C and 118 mm of rain, in part due to an extended heat wave during the 2015 summer. For both years, the below-canopy PPFD was approximately 20% of the above-canopy PPFD before canopy leaf emergence and less than 1% under full canopy closure (Figure 1a). Below-canopy mean air temperatures were consistently warmer than above-canopy, with a difference of on average 2.2 °C during the two years (Figure 1b). Soil temperatures in July-August were on average 2.7 °C warmer in 2015 as compared to 2014 due to the warmer temperatures and reduced soil water content during the 2015 growing season (Figure 1c). Soil water content decreased to 10% in July 2015 and remained low for the rest of the summer (Figure 1d) due to the lack of precipitation. Below and above-canopy air temperatures became similar as the dry conditions persisted in 2015, probably due to a reduction in evapotranspiration and an increase in sensible heat flux, common for ecosystems under drought stress (e.g. Teuling et al., 2010; Wolf et al., 2013; Wolf et al., 2016). The prevailing wind directions above the canopy were aligned on slope parallel to the ridge of the Lägeren mountain range in the West to East direction (Figure 2). Below-canopy wind directions followed a similar distribution to the above-canopy wind directions, but with a deflection angle of approximately 30° towards the South.

The development of overstory and understory leaf area index (LAI) during the 2015 growing season at Lägeren differed between the two canopy layers (Figure 3). Overstory LAI

14

319 increased considerably from April (2 m^2 m^{-2}) to late May (6 m^2 m^{-2}), with the emergence of the

320 deciduous canopy leaves. Understory LAI, predominantly composed of *Allium ursinum*, started

321 growing in March before full canopy leaf-out (second half of April to first half of May), taking

322 advantage of the high light availability in the understory during this period (Figure 1a).

323 Understory LAI, and associated understory biomass, increased until late May and then decreased

324 rapidly as *Allium ursinum* underwent senescence under full canopy closure (Figure 3b).

325 Afterwards, only a few sparse plants of *Hedera helix* L. and *Lamium galeobdolon* (L.) L. s.l.

326 were able to grow in the understory as well as a few seedlings and saplings.

327

3.2 Measured below-canopy CO$_2$ fluxes

329   On an annual basis, the below canopy was a strong net source of carbon (NEP$_{below}$= − 647

330 ± 65 g C m^{-2} yr^{-1}) (Table 1). Below-canopy carbon losses were larger in 2014 than in 2015

331 (Figure 4a), probably due to limitations on soil respiration due to dry soil conditions in 2015

332 (Figure 1d), as previous studies have shown a reduction in soil respiration at the Lägeren site for

333 soil water content below 15% (Ruehr et al., 2010). Understory vegetation and soil were a net

334 sink of carbon only in spring, with the early emergence of the wild garlic (*Allium ursinum*)

335 before canopy leaf-out (Figure 3), while it was a net source of carbon for the rest of the year,

336 particularly in summer and fall (Figure 4a). Understory GPP (Figure 4b) depended both on

337 weather conditions and tree canopy cover. The phenological escape of understory plants

338 (Crawley, 2009), i.e., when understory plants reach their maximum LAI or photosynthetic rates

339 before overstory canopy closure, was observed during both years in spring (Figure 3). Spring

340 escape is a common adaptation strategy of understory plants, taking advantage of a short-time

341 period with spring warming and high light availability before tree canopy foliage emergence

342   (Crawley, 2009; Mahall and Bormann, 1978; Sparling, 1967), as seen for the wild garlic at the

343   Lägeren site (Figure 3b). During summer 2014, below-canopy GPP was linked to the

344   combination of understory plant species, understory trees, and overstory trees with lower

345   branches below the overstory canopy. In fall, overstory canopy opening only occurred later in

346   October or November when temperatures were colder and the forest floor was covered with a

347   thick layer of dead leaves, thereby inhibiting understory photosynthesis. High respiration rates (~

348   5 $\mu mol\ m^{-2}\ s^{-1}$) in the understory were found in summer at high temperatures with sufficient

349   water availability, and after senescence in fall, when temperatures were high enough (> 5 °C) to

350   allow microbial litter decomposition, especially from the nutrient-rich dead deciduous leaves on

351   the soil surface (Figure 4c). During summer and fall 2015, the soil was warmer (+2.7°C on

352   average) and dryer (<12%) compared to 2014 (Figure 1) due to a long-lasting drought and heat

353   wave. Consequently, soil respiration processes were limited, as can be seen in the reduced

354   below-canopy R for August to November 2015 compared to 2014 (Figure 4c). These reductions

355   measured by the below-canopy EC system are in agreement with those measured in previous

356   years at the site by Ruehr et al. (2010). These dry conditions also led to lower GPP (Figure 4b)

357   and autotrophic respiration below canopy in summer 2015 compared to 2014.

358   Previous studies have found a similar consistent seasonal pattern, as seen in Figure 4c, in

359   the magnitude of soil respiration over the years at Lägeren, ranging from a minimum of about 0.5

360   $\mu mol\ m^{-2}\ s^{-1}$ in winter to a maximum of about 5.5 $\mu mol\ m^{-2}\ s^{-1}$ in summer (Etzold et al., 2011;

361   Ruehr et al., 2010). The average below-canopy R over the two years (769 ± 130 g C $m^{-2}\ yr^{-1}$)

362   (Table 1) agreed well with the average soil respiration measured by chambers over four years

363   (890 ± 46 g C $m^{-2}\ yr^{-1}$) (Etzold et al., 2011; Ruehr et al., 2010). Lower annual below-canopy R

364   was found in 2015 due to the dry conditions (639 g C $m^{-2}\ yr^{-1}$) compared to wetter conditions in

16

365   2014 (898 C m^{-2} yr^{-1}). As below-canopy R was similar to average soil respiration (Ruehr et al.,

366   2010), this suggested that most of the below-canopy R came from the soil. Overall, despite the

367   possible challenges linked to partitioning below-canopy fluxes, the agreement between the soil

368   respiration measured and below-canopy R showed the feasibility of below-canopy flux

369   partitioning at the Lägeren site. While at some sites common methods for calculating fluxes from

370   below-canopy measurements are impeded by the low turbulence and require different methods

371   (e.g. Jocher et al., 2017), other below-canopy sites also reported suitable turbulence conditions to

372   partition below-canopy EC fluxes based on common methods (Black et al., 1996; Misson et al.,

373   2007).

374

375   **3.3   Measured above-canopy CO$_2$ fluxes**

376   The above-canopy fluxes were, in comparison to the below-canopy fluxes, a net carbon

377   sink (NEP$_{above}$) during most of the year in 2014 and 2015 (Figure 4a). Above-canopy fluxes were

378   a small net source of carbon in winter and transitioned to a net sink in summer. High

379   photosynthesis rates were found in late spring/summer due to favorable light conditions,

380   sufficient water supply and high temperatures, as the deciduous trees gradually started to become

381   active in the second half of May until senescence in October (Figure 3a; Figure 4b). Given that

382   temperatures are high enough, the evergreen trees at the Lägeren site can photosynthesize during

383   most of the year (including winter). This can be seen by the low, but still present, photosynthesis

384   rates in winter (Figure 4b). However, above-canopy respiratory fluxes were unexpectedly low in

385   summer under full canopy cover (Figure 4c). Respiratory fluxes at Lägeren decreased after full

386   canopy leaf-out in the second half of May 2014 and 2015, when they would have been expected

387   to increase due to higher temperatures (higher heterotrophic respiration) and more active biomass

17

388   respiring (higher autotrophic respiration) (Figure 4c). Respiratory fluxes increased again after

389   leaf senescence in fall. The respiration partitioned from above-canopy measurements was also

390   smaller than that partitioned from the below-canopy measurements during the growing seasons

391   (Figure 4c). Moreover, annual NEP_{above} was on average 758 ± 10 g C m^{-2} yr^{-1} over the two years

392   (Table 1), which is well outside the range reported for comparable temperate deciduous forests

393    $(311 \pm 38$ g C m^{-2} $yr^{-1})$ or evergreen forests $(398 \pm 42$ g C m^{-2} $yr^{-1})$ (Luyssaert et al., 2007).

394   Storage fluxes estimated at 3 g C m^{-2} yr^{-1} were found to have only a small influence on annual

395   NEP_{above}. These observations, in combination with the previous study by Etzold et al. (2010),

396   suggested that some fluxes from the below canopy were not accounted for in the above-canopy

397   measurements, which prompted further investigation on a potential decoupling of below and

398   above-canopy fluxes.

399

3.4   Evidence for decoupling

401   Profile measurements were used to investigate the presence of a decoupling of the below

402   and above-canopy layers, independently of the EC measurements. The profile measurements

403   showed that the largest gradients in CO_2 concentrations throughout the profile occurred during

404   summer (Figure 5a). CO_2 concentration gradients along the 54 m profile were smallest in winter

405   (5 ppm), increased in spring (10 ppm) and reached a maximum in summer (30 ppm) to finally

406   decrease again in fall with canopy leaf senescence (20 ppm). Although higher CO_2

407   concentrations are to be expected near the soil surface in summer due to enhanced soil

408   respiration, these high concentrations were seen only in the lower part of the profile. Only at 9 m

409   height and above were CO_2 concentrations similar to those at the top of the canopy, well mixed

410   with background air as expected (Buchmann et al., 1998; Buchmann et al., 1996). Thus, the high

18

411   CO_2 concentration layer extended from near the surface to at least 5 m height (but < 9 m). These

412   high CO_2 concentrations moved horizontally with the drainage flow along the surface (as

413   indicated in Figure 2 by the wind directions below the canopy) rather than vertically, particularly

414   during the main growing season. This interpretation is also supported by the within canopy wind

415   speed measurements: wind speed was highest above the canopy, decreased within the canopy

416   layer, but increased again below 10 m towards the surface (Figure 5d), indicating horizontal

417   pressure gradient forces (e.g. Kaimal and Finnigan, 1994) leading to the decoupled below-

418   canopy layer. Similar profiles were found for daytime and nighttime (see supplementary Figure S

419   2).

420   The relationship between the standard deviation of the vertical wind velocity (σ_w) below

421   and above-canopy was also used to investigate for decoupling (Jocher et al., 2017; Thomas et al.,

422   2013). The relationship between σ_w below and above-canopy was more linear, as shown by the

423   higher goodness of fit and less scatter, in spring ($R^2_{raw} = 0.40$, $R^2_{bin} = 0.76$) and winter ($R^2_{raw} = 0.33$,

424    $R^2_{bin} = 0.28$) compared to summer ($R^2_{raw} = 0.05$, $R^2_{bin} = 0.10$) and fall ($R^2_{raw} = 0.05$, $R^2_{bin} = 0.003$) when

425   no clear relationships could be found due to the large scatter (Figure **6**). These results suggested

426   that the two layers at the Lägeren forest were coupled in spring and winter and were decoupled

427   in summer and fall. Interestingly, below-canopy σ_w values during decoupled months tended to

428   be similar or higher than during coupled months (Figure **6**). This is unusual given that

429   decoupling is in general found in forests during stable nocturnal periods with low turbulence

430   (e.g. Alekseychik et al., 2013; Belcher et al., 2008; van Gorsel et al., 2011). A 5-day moving

431   window approach was used to identify decoupled periods. Using 5 days of data allowed having

432   enough points to investigate the relationships, while it also considerably reduced the scatter

433 shown for the seasons in Figure 6, with greater goodness of fit for coupled periods ($R^2_{raw} = 0.76$,

434 $R^2_{bin} = 0.93$) compared to decoupled periods ($R^2_{raw} = 0.17$, $R^2_{bin} = 0.32$) (Figure 7). Based on the 5-

435 day moving window approach, the decoupled periods during the two years of measurements

436 were from June 1 to October 14 in 2014 and from May 20 to October 14 in 2015 (± 2 days for all

437 dates). These decoupled periods corresponded to periods with full canopy cover, as determined

438 using the phenological camera on top of the EC tower and the LAI measurements, from June 1 to

439 October 15 in 2014, and from May 20 to October 15 in 2015. The onset of these periods

440 coincided with a sharp and constant reduction in above-canopy R (spring), while an increase in

441 above-canopy R (fall) indicated the end of the decoupled period. It is important to note that

442 decoupling does not stop when above-canopy photosynthesis declines, but rather when the leaves

443 have fallen, which can be more than a month after the above-canopy deciduous leaves have

444 become senescent.

445   During the decoupled periods, the mean directional wind shear between below and

446 above-canopy was also found to increase past the 70° threshold (see supplementary Figure S 3).

447 Although in some studies wind shear can be directly linked to decoupling (e.g. Alekseychik et

448 al., 2013), the wind shear was not consistently linked to decoupling at the Lägeren site (see

449 supplementary Figure S 3). Several studies have associated decoupling to stable conditions (e.g.

450 Alekseychik et al., 2013; van Gorsel et al., 2011). However, after testing with turbulent kinetic

451 energy (see supplementary Figure S 4) and with Richardson numbers (see supplementary Figure

452 S 5), it was found that decoupling at the Lägeren site could not be defined based on stability

453 based indices as it also occurred during unstable, turbulent daytime conditions.

454

3.5   Decoupling and advection at the Lägeren site

455   **3.5   Decoupling and advection at the Lägeren site**

456   Etzold et al. (2010) estimated the influence of advection for the ecosystem CO_2 flux

457   measured at the Lägeren site to be 36% for the period from May to August 2007 using a two-

458   dimensional approach along the slope with profile measurements. They estimated that the forest

459   fixed 157 g C m^{-2} less than what the direct EC measurements above the canopy suggested for

460   these four months. Several studies have shown that the filtering of low turbulence periods (low

461   u_*) results in a systematic decrease in annual NEP, which can range from 50 to 200 g C m^{-2} yr^{-1}

462   (Carrara et al., 2003; Falge et al., 2001; Hui et al., 2004; Papale et al., 2006). Following this line

463   of argumentation, a u_*-threshold of 0.30 m s^{-1} was suggested by Etzold et al. (2010) to account

464   for periods with advection at this site, leading to an increase in respiration of 107 g C m^{-2} and

465   consequently, to a decrease in NEP by the same amount. Although filtering with a u_*-threshold is

466   often used as the best practice to deal with advection, it only accounted for 2/3 of the advection

467   flux empirically estimated from horizontal and vertical gradient measurements during the four

468   months of direct comparison by Etzold et al. (2010).

469   In this study, u_*-filtering was not used to enable a detailed investigation of the measured

470   contributions of below and above-canopy fluxes, and also because the decoupling was not

471   confined to periods of low turbulence at night. In addition, the common methods for determining

472   the u_*-threshold (e.g. Goulden et al., 1997; Gu et al., 2005) cannot be used at the Lägeren site as

473   they do not detect a threshold, i.e., there is no inflection point. Instead, the integral turbulence

474   criterion test (Foken et al., 2005) and other quality filtering (see Section 2.6.1) were used to

475   ensure of the quality of the fluxes. Above-canopy u_*-values were relatively high for both years at

476   Lägeren, with most values being in the range of 0.40-0.45 m s^{-1} during nighttime and in the range

477 of 0.45-0.60 m s^{-1} during daytime, indicating good turbulent mixing even at night. The

478 discrepancy therefore seemed to lie in the fluxes actually reaching the EC system above canopy

479 and not primarily in low turbulence conditions *per se*.

480 The below-canopy EC measurements at Lägeren provided crucial additional insights to

481 better understand these carbon dynamics and a potential decoupling of below and above-canopy

482 fluxes. The uncommonly large measured annual NEP_{above} and the reduction in R_{above} during the

483 growing season, as well as the additional investigations they prompted, indicated that starting

484 with full canopy closure in the second half of May/beginning of June, a decoupling between

485 below and above-canopy fluxes occurred (Figure 4c). As the annual below-canopy fluxes at

486 Lägeren are dominated by respiration (except during spring), this led to an overestimation of

487 annual ecosystem NEP (758 ± 10 g C m^{-2} yr^{-1}) and a large underestimation of ecosystem R (494

488 ± 5 g C m^{-2} yr^{-1}), while GPP was only slightly affected (1252 ± 5 g C m^{-2} yr^{-1}) (Figure 4 and

489 Table 1). The decoupling influence was also greater in 2014 than in 2015 due to the greater

490 influence of soil respiration (Figure 4c and Table 1).

491 Below-canopy air masses in a forest can be affected by the local topography, thus

492 resulting in a horizontal exchange along the surface (Belcher et al., 2008; Belcher et al., 2012).

493 Decoupling is therefore often associated with nighttime conditions, as turbulence within the

494 canopy collapses under stable stratification, while the flow above canopy remains turbulent

495 (Belcher et al., 2008). The air within the canopy then creates downslope drainage currents,

496 thereby not reaching the EC measurements above canopy (Aubinet et al., 2005; Belcher et al.,

497 2008; Feigenwinter et al., 2004; Staebler and Fitzjarrald, 2004). Despite the predominance of

498 decoupling during nighttime at most sites (e.g. Alekseychik et al., 2013; van Gorsel et al., 2011),

499 some sites are also affected by decoupling during daytime due to the influence of local

22

500   topography (Jocher et al., 2017) or of a dense canopy cover (Thomas et al., 2013). At the

501   Lägeren site, the tree canopies created a mechanical barrier, which led to decoupled flow layers

502   below and above this barrier; the scalars (e.g. CO_2) that remain in the below-canopy layer could

503   then be advected away. Consequently, the below-canopy fluxes were not fully measured by the

504   above-canopy EC system in 2014 and 2015. Under decoupled conditions, NEP based on above-

505   canopy measurements does not reflect the entire ecosystem, but rather the upper layer, i.e., the

506   tree canopies. As a result, decoupling often results in a considerable overestimation of above-

507   canopy NEP, as below-canopy fluxes, which are dominated by R, are advected away from the

508   ecosystem without being measured (Goulden et al., 1996; Thomas et al., 2013).

509

510   **3.6   Correcting above-canopy CO_2 fluxes for decoupling**

511   Thomas et al. (2013) suggested a correction for decoupled subcanopies that consisted of

512   adding the below-canopy fluxes, which in their study were only composed of soil respiration

513   (i.e., no understory vegetation), to the above-canopy fluxes during decoupled periods. The

514   subcanopy correction decreased the unrealistically high NEP_{above} of 1100 g C m^{-2} yr^{-1} for their

515   forest in Oregon to a more realistic 480 g C m^{-2} yr^{-1}. At Lägeren, the decoupling was observed

516   under full canopy closure, i.e. when all deciduous leaves were out, and thus, the missing above-

517   canopy fluxes were recovered using the decoupling correction approach from Thomas et al.

518   (2013) during the identified decoupled periods. As some understory plants are present at the

519   Lägeren site, this decoupling correction implied adding the net fluxes from the below canopy,

520   composed of both below-canopy R and understory GPP, to the above-canopy fluxes when the

521   measurements from the two layers were decoupled. As the decoupling and associated drainage

522   flow at the Lägeren site occurs within the lower 9 m of the tree trunks (Figure 5), it could

23

523 therefore be assumed that R and GPP occurring within the tree canopy remained unaffected by

524 the drainage flow and were accurately measured by the above-canopy EC system.

525   The decoupling correction resulted in a large increase in R_{above} and associated decrease in

526 NEP_{above}, while GPP_{above} was only slightly increased (Figure 8). Following the correction, R_{above}

527 increased during the growing season, as would be expected with the higher temperatures and

528 greater biomass respiring (Figure 8c). R_{above} followed similar trends as R_{below}, being on average 1

529 to 2 µmol m^{-2} s^{-1} greater. R_{above} reached a maximum of about 7 µmol m^{-2} s^{-1} in July-August, when

530 R_{below} also reached a maximum of about 5 µmol m^{-2} s^{-1}. A secondary maximum in both R_{above} and

531 R_{below} was observed in 2014 due to the decomposition of dead deciduous leaves on the soil

532 surface (Figure 8c), as temperature and soil water content were not limiting (Figure 1). However,

533 this secondary maximum in R was not seen in 2015 due to low soil water content (~12%) which

534 lasted until November 2015 (Figure 1d). In addition, the decoupling correction also led to a small

535 increase of 3% in energy balance closure when added to the sensible and latent heat fluxes (see

536 supplementary Figure S 6).

537

538 **3.7   Comparison of functional relationships for uncorrected and corrected fluxes**

539   Uncorrected above-canopy respiration increased with soil temperature, but levelled off at

540 about 2 µmol m^{-2} s^{-1} (Table 2) when soil temperatures were 5-6 °C in 2014 and 2015 (Figure 9).

541 In contrast, below-canopy respiration increased exponentially with temperature until respiration

542 reached about 4 µmol m^{-2} s^{-1} at 12°C in 2014 and 14 °C in 2015, before levelling off (Figure 9)

543 when soil water content became limiting. This interpretation is supported by the fact that during

544 the entire year, the below-canopy respiration was mostly coming from the soil (Etzold et al.,

545 2011; Ruehr et al., 2010) and thus, it was strongly affected by temperature, soil volumetric water

24

546   content (summer) and substrate availability (e.g., dead leaves in fall) (Figure 4c). Applying the

547   decoupling correction allowed recovery of the below-canopy R that was missing from above-

548   canopy R and sharply increased the goodness of fit as well (Table 2). After the correction, above-

549   canopy R increased exponentially with temperature, reflecting both the effect of increasing

550   autotrophic respiration from the living biomass and heterotrophic respiration from decomposition

551   (Figure 9).

552   Compared to R, the effect of the decoupling correction on GPP was much smaller, as the

553   annual below-canopy fluxes were dominated by respiration, except for a short period in

554   spring/early summer (Figure 4). GPP did not change substantially following the correction

555   (Figure 10), especially in 2015 when below-canopy GPP was very low with 57 g C m^{-2} yr^{-1}

556   compared to 187 g C m^{-2} yr^{-1} in 2014 (Table 1). This was also shown by very similar quantum

557   yields as well as R^2 values, although slightly lower due to the inclusion of understory vegetation,

558   for corrected *vs*. uncorrected above-canopy GPP data (Table 3). Below-canopy GPP was

559   constrained by PPFD in 2014 as there was still GPP during the summer under low light

560   conditions, while in 2015 below-canopy GPP was mostly during the high light conditions in

561   spring (Figure 4b). Consequently, the understory vegetation showed a typical hyperbolic

562   relationship with PPFD in 2014, saturating at about 2 μmol m^{-2} s^{-1} (Table 3), but did not saturate

563   as much in 2015.

564

565   **3.8   Implications for carbon budget at the Lägeren site**

566   Adding the below-canopy fluxes to the above-canopy fluxes led to a decrease in overall

567   carbon uptake (NEP) from the site. The decoupling correction reduced the average annual

568   NEP$_{above}$ from 758 ± 10 g C m^{-2} yr^{-1} to 327 ± 4 g C m^{-2} yr^{-1}, mostly by increasing R (see Table 1).

569 After leaf emergence, below and above-canopy NEP distinctly diverged because of CO_2

570 assimilation by the overstory while below-canopy respiration increased (Figure 8), similar to

571 what was found previously in deciduous forests (Black et al., 1996). Positive above-canopy NEP

572 showed the carbon uptake of the system as a whole, while negative below-canopy NEP showed

573 the release of carbon. In the synthesis study by Misson et al. (2007), eight of the eleven below-

574 canopy sites studied were also sources of carbon during summer. The correction of the above-

575 canopy fluxes during the decoupled period led to an increase in R_{above} of 50% in 2014 and of

576 48% in 2015 (Table 1). Overall, GPP_{below} contributed only 9% to GPP_{above}, while R_{below}

577 contributed 79% to R_{above} (Table 1). These average relative flux contributions from the Lägeren

578 below-canopy layer were within the ranges reported from previous studies, with 0 to 39% for

579 GPP and 32 to 79% for R (Misson et al., 2007). The contribution from GPP_{below} at Lägeren was

580 lower than the average of 14% found by Misson et al. (2007), probably because Lägeren is a

581 dense forest with a relatively high LAI, while the contribution from R_{below} was above the average

582 of 55%.

583   Moreover, following the decoupling correction, NEP_{above} agreed well with NEP estimates

584 derived from allometric functions using biomass inventory data combined with models for

585 respiration ($NEP_{biomass}$= 331±10 g C m^{-2} yr^{-1}). In a previous study by Etzold et al. (2011),

586 $NEP_{biomass}$ was estimated at 307 g C m^{-2} yr^{-1} (296 to 319 g C m^{-2} yr^{-1}) based on data from 2005 and

587 2009. Biomass inventory data from 2015 indicated that trees grew on average 8% since 2005 and

588 5% since 2009, leading to a $NEP_{biomass}$ from allometric functions of 321 to 341 g C m^{-2} yr^{-1}. These

589 results therefore suggest that the decoupling correction was effective in recovering the part of the

590 flux which was not measured above-canopy and led to NEP values close to independent NEP

591 estimates for the site as well as to other temperate deciduous forests comparable to Lägeren

26

592　(Luyssaert et al., 2007). Indeed, average annual NEP (327 ± 4 g C m^{-2} yr^{-1}), GPP (1297 ± 28 g C

593　m^{-2} yr^{-1}) and R (970 ± 25 g C m^{-2} yr^{-1}) at Lägeren in 2014 and 2015, were well within the ranges

594　recorded for similar temperate deciduous forests for NEP (311 ± 38 g C m^{-2} yr^{-1}), GPP ($1375 \pm$

595　56 g C m^{-2} yr^{-1}) and R (1048 ± 64 g C m^{-2} yr^{-1}) (Figure 11).

596　　　　In comparison, although the approach from Etzold et al. (2010) helped in reducing the

597　annual NEP in 2014 and 2015, NEP was still higher than our corrected NEP estimates with $536 \pm$

598　35 g C m^{-2} yr^{-1} when using the u_*-filtering and with 484 ± 7 g C m^{-2} yr^{-1} when removing 36%

599　advection (Table 4). Moreover, u_*-filtering did not fully resolve the decoupling problem (see

600　supplementary Figure S 7), as it is only applied to low turbulence conditions at night whereas

601　decoupling also occurred under turbulent conditions, while the 36% advection correction can

602　only be applied to annual sums and cannot correct the high-resolution flux time series available.

603　Other studies have also shown that the u_*-threshold can be insufficient in accounting for

604　advection or is not necessarily a good indicator for below-canopy turbulence (Jocher et al., 2017;

605　Speckman et al., 2015; van Gorsel et al., 2011).

606　　　　Although the goal of the decoupling correction was to obtain more reliable net CO_2

607　exchange estimates, it should be noted that the correction bears the risk of double accounting if

608　some eddies would eventually reach the above-canopy EC system. However, these net ecosystem

609　carbon budgets are the best available direct estimates of the ecosystem CO_2 exchange, given the

610　challenging measurement conditions for complex forest sites such as Lägeren. For our site, the

611　decoupling correction reduced the high NEP estimates to a range closer to biomass-derived NEP

612　for the site, indicating a successful accounting for the decoupling. Although the uncertainties in

613　the corrected NEP estimates are difficult to quantify, such uncertainties are inherent to sites with

614   considerable advection (Kutsch et al., 2008) given the complexity of the problem and that even

615   with extensive advection measurements, it is difficult to fully quantify its magnitude (Aubinet et

616   al., 2010).

617

618   **3.9   Importance of below-canopy measurements**

619   Decoupling is present to varying extents at diverse EC sites and its effect on measured net

620   ecosystem carbon budget is often unknown until additional measurements are performed. Below-

621   canopy EC measurements can provide unique insights on below-canopy carbon dynamics and

622   turbulence, which are often lacking when relying only on above-canopy EC measurements and

623   thereby, can help improve the accuracy of forest carbon budgets. In extreme cases, below-canopy

624   measurements can enable realistic NEP estimates for forests known to be completely decoupled

625   due to dense canopy covers (Thomas et al., 2013). In some cases, below-canopy measurements

626   will help resolve inconsistencies such as winter uptake in measured above-canopy fluxes (e.g.

627   Jocher et al., 2017). In many other cases, such as Tota et al. (2008) and this study, below-canopy

628   measurements will complement the above-canopy measurements in a way that could not have

629   been predicted otherwise and allow a more accurate NEP estimation for the site. It is however

630   important to note that below-canopy fluxes can unfortunately not be derived at all sites due to the

631   low turbulence conditions making the EC flux calculations impossible. However, even in such

632   cases, alternative methods such as the conditional sampling method (Desjardins, 1977; Thomas

633   et al., 2008) can be used to estimate the flux. The common practice in the flux community to

634   account for decoupling or advection by filtering based on above-canopy u_*-threshold has been

635   shown to be ineffective at many sites (e.g. Acevedo et al., 2009; Jocher et al., 2017; Speckman et

636   al., 2015; van Gorsel et al., 2011) and below-canopy measurements can offer the solution needed

637   at some of these sites.

638

639   **4.   Conclusions**

640   Concurrent below and above-canopy EC measurements captured the very different

641   carbon dynamics of the respective layers well: while the above canopy was a net carbon sink, the

642   below canopy was a net source during most of the year, except in spring. Below and above-

643   canopy fluxes were decoupled during the growing season, resulting in a large overestimation of

644   the measured net ecosystem-scale carbon uptake for this mixed forest site. The measurements of

645   below-canopy fluxes enabled the correction of this overestimation, and corrected ecosystem

646   fluxes agreed well with independently estimated NEP from biomass inventories combined with

647   models. Our results clearly demonstrated that below-canopy EC measurements are essential in

648   this mixed forest, and likely in many other forests, to gain reliable estimates of the CO_2 exchange

649   in structurally complex forest ecosystems.

650

663 **References**

664 Acevedo, O.C. et al., 2009. Is friction velocity the most appropriate scale for correcting nocturnal
665   carbon dioxide fluxes? Agricultural and Forest Meteorology, 149(1): 1-10.
666 Ahrends, H.E. et al., 2008. Quantitative phenological observations of a mixed beech forest in
667   northern Switzerland with digital photography. J Geophys Res-Biogeo, 113(G4).
668 Alekseychik, P., Mammarella, I., Launiainen, S., Rannik, U. and Vesala, T., 2013. Evolution of
669   the nocturnal decoupled layer in a pine forest canopy. Agricultural and Forest
670   Meteorology, 174: 15-27.
671 Assmann, S.M., 1986. Zur theorie der grundflächenhaltung. Forstwiss Centralblatt, 87: 1368-
672   1378.
673 Aubinet, M. et al., 2005. Comparing CO_2 storage and advection conditions at night at different
674   CarboEuroflux sites. Boundary-Layer Meteorology, 116(1): 63-94.
675 Aubinet, M. et al., 2010. Direct advection measurements do not help to solve the night-time CO_2
676   closure problem: Evidence from three different forests. Agricultural and Forest
677   Meteorology, 150(5): 655-664.
678 Baldocchi, D.D., 2003. Assessing the eddy covariance technique for evaluating carbon dioxide
679   exchange rates of ecosystems: Past, present and future. Global change biology, 9(4): 479-
680   492.
681 Baldocchi, D.D. and Vogel, C.A., 1996. Energy and CO_2 flux densities above and below a
682   temperate broad-leaved forest and a boreal pine forest. Tree Physiol, 16(1-2): 5-16.
683 Baldocchi, D.D., Vogel, C.A. and Hall, B., 1997. Seasonal variation of carbon dioxide exchange
684   rates above and below a boreal jack pine forest. Agricultural and Forest Meteorology,
685   83(1-2): 147-170.
686 Barr, A.G. et al., 2004. Inter-annual variability in the leaf area index of a boreal aspen-hazelnut
687   forest in relation to net ecosystem production. Agricultural and Forest Meteorology,
688   126(3-4): 237-255.
689 Belcher, S.E., Finnigan, J.J. and Harman, I.N., 2008. Flows through forest canopies in complex
690   terrain. Ecol Appl, 18(6): 1436-1453.
691 Belcher, S.E., Harman, I.N. and Finnigan, J.J., 2012. The wind in the willows: flows in forest
692   canopies in complex terrain. Annu Rev Fluid Mech, 44: 479-504.
693 Black, T.A. et al., 1996. Annual cycles of water vapour and carbon dioxide fluxes in and above a
694   boreal aspen forest. Global change biology, 2(3): 219-229.
695 Buchmann, N., Hinckley, T.M. and Ehleringer, J.R., 1998. Carbon isotope dynamics in *Abies*
696   *amabilis* stands in the Cascades. Can J Forest Res, 28(6): 808-819.
697 Buchmann, N., Kao, W.Y. and Ehleringer, J.R., 1996. Carbon dioxide concentrations within
698   forest canopies - Variation with time, stand structure, and vegetation type. Global change
699   biology, 2(5): 421-432.
700 Burns, S.P. et al., 2011. Atmospheric stability effects on wind fields and scalar mixing within
701   and just above a subalpine forest in sloping terrain. Boundary-Layer Meteorology,
702   138(2): 231-262.
703 Carrara, A. et al., 2003. Net ecosystem CO_2 exchange of mixed forest in Belgium over 5 years.
704   Agricultural and Forest Meteorology, 119(3-4): 209-227.

705 Constantin, J., Grelle, A., Ibrom, A. and Morgenstern, K., 1999. Flux partitioning between
706   understorey and overstorey in a boreal spruce/pine forest determined by the eddy
707   covariance method. Agricultural and Forest Meteorology, 98-9: 629-643.
708 Cook, B.D. et al., 2004. Carbon exchange and venting anomalies in an upland deciduous forest
709   in northern Wisconsin, USA. Agricultural and Forest Meteorology, 126(3-4): 271-295.
710 Crawley, M.J., 2009. Life History and Environment, Plant Ecology. Blackwell Publishing Ltd.,
711   pp. 73-131.
712 de Wit, H.A., Palosuo, T., Hylen, G. and Liski, J., 2006. A carbon budget of forest biomass and
713   soils in southeast Norway calculated using a widely applicable method. Forest Ecology
714   and Management, 225(1-3): 15-26.
715 Desjardins, R.L., 1977. Description and evaluation of a sensible heat flux detector. Boundary-
716   Layer Meteorology, 11(2): 147-154.
717 Ernst, W.H.O., 1979. Population biology of *Allium ursinum* in northern Germany. J Ecol, 67(1):
718   347-&.
719 Etzold, S., Buchmann, N. and Eugster, W., 2010. Contribution of advection to the carbon budget
720   measured by eddy covariance at a steep mountain slope forest in Switzerland.
721   Biogeosciences, 7(8): 2461-2475.
722 Etzold, S. et al., 2011. The carbon balance of two contrasting mountain forest ecosystems in
723   Switzerland: Similar annual trends, but seasonal differences. Ecosystems, 14(8): 1289-
724   1309.
725 Falge, E. et al., 2001. Gap filling strategies for defensible annual sums of net ecosystem
726   exchange. Agricultural and Forest Meteorology, 107(1): 43-69.
727 Falk, M., Wharton, S., Schroeder, M., Ustin, S. and U, K.T.P., 2008. Flux partitioning in an old-
728   growth forest: Seasonal and interannual dynamics. Tree Physiol, 28(4): 509-520.
729 Feigenwinter, C., Bernhofer, C. and Vogt, R., 2004. The influence of advection on the short term
730   CO_2-budget in and above a forest canopy. Boundary-Layer Meteorology, 113(2): 201-
731   224.
732 Finnigan, J.J., Clement, R., Malhi, Y., Leuning, R. and Cleugh, H.A., 2003. A re-evaluation of
733   long-term flux measurement techniques part I: Averaging and coordinate rotation.
734   Boundary-Layer Meteorology, 107(1): 1-48.
735 Foken, T. et al., 2005. Post-field data quality control. In: X. Lee, W. Massman and B. Law
736   (Editors), Handbook of Micrometeorology. Atmospheric and Oceanographic Sciences
737   Library. Springer Netherlands, pp. 181-208.
738 Foken, T. et al., 2012. Coupling processes and exchange of energy and reactive and non-reactive
739   trace gases at a forest site - results of the EGER experiment. Atmos Chem Phys, 12(4):
740   1923-1950.
741 Göckede, M. et al., 2008. Quality control of CarboEurope flux data - Part 1: Coupling footprint
742   analyses with flux data quality assessment to evaluate sites in forest ecosystems.
743   Biogeosciences, 5(2): 433-450.
744 Goulden, M.L. et al., 1997. Physiological responses of a black spruce forest to weather. J
745   Geophys Res-Atmos, 102(D24): 28987-28996.
746 Goulden, M.L., Munger, J.W., Fan, S.-M., Daube, B.C. and Wofsy, S.C., 1996. Measurements of
747   carbon sequestration by long-term eddy covariance: methods and a critical evaluation of
748   accuracy. Global change biology, 2: 169-182.

749 Gu, L.H. et al., 2005. Objective threshold determination for nighttime eddy flux filtering.
750   Agricultural and Forest Meteorology, 128(3-4): 179-197.
751 Horst, T.W., 1997. A simple formula for attenuation of eddy fluxes measured with first-order-
752   response scalar sensors. Boundary-Layer Meteorology, 82(2): 219-233.
753 Hui, D.F. et al., 2004. Gap-filling missing data in eddy covariance measurements using multiple
754   imputation (MI) for annual estimations. Agricultural and Forest Meteorology, 121(1-2):
755   93-111.
756 Janssens, I.A., Kowalski, A.S. and Ceulemans, R., 2001. Forest floor CO_2 fluxes estimated by
757   eddy covariance and chamber-based model. Agricultural and Forest Meteorology, 106(1):
758   61-69.
759 Jocher, G. et al., 2017. Apparent winter CO_2 uptake by a boreal forest due to decoupling.
760   Agricultural and Forest Meteorology, 232: 23-34.
761 Jones, H.G., 2014. Plants and Microclimate: A Quantitative Approach to Environmental Plant
762   Physiology. Cambridge University Press, 423 pp.
763 Kaimal, J.C. and Finnigan, J.J., 1994. Atmospheric Boundary Layer Flows: Their Structure and
764   Measurement. Oxford University Press.
765 Kaimal, J.C., Izumi, Y., Wyngaard, J.C. and Cote, R., 1972. Spectral characteristics of surface-
766   layer turbulence. Q J Roy Meteor Soc, 98(417): 563-589.
767 Kaufmann, E., 2001. Estimating of standing timber, growth and cut. In: P. Brassel and H.
768   Lischke (Editors), Swiss National Forest Inventory: methods and models of the second
769   assessment. Birmensdorf: Swiss Federal Institute WSL, pp. 162-196.
770 Kutsch, W.L. et al., 2008. Advection and resulting CO_2 exchange uncertainty in a tall forest in
771   central Germany. Ecol Appl, 18(6): 1391-1405.
772 Larcher, W., 2003. Physiological Plant Ecology: Ecophysiology and Stress Physiology of
773   Functional Groups. Springer, Berlin, Germany.
774 Launiainen, S. et al., 2005. Eddy covariance measurements of CO_2 and sensible and latent heat
775   fluxes during a full year in a boreal pine forest trunk-space. Boreal Environ Res, 10(6):
776   569-588.
777 Law, B.E., Baldocchi, D.D. and Anthoni, P.M., 1999. Below-canopy and soil CO_2 fluxes in a
778   Ponderosa pine forest. Agricultural and Forest Meteorology, 94(3-4): 171-188.
779 Law, B.E. et al., 2001. Spatial and temporal variation in respiration in a young Ponderosa pine
780   forests during a summer drought. Agricultural and Forest Meteorology, 110(1): 27-43.
781 Luyssaert, S. et al., 2007. CO_2 balance of boreal, temperate, and tropical forests derived from a
782   global database. Global change biology, 13(12): 2509-2537.
783 Mahall, B.E. and Bormann, F.H., 1978. Quantitative description of the vegetative phenology of
784   herbs in a northern hardwood forest. Bot Gaz, 139(4): 467-481.
785 Misson, L. et al., 2007. Partitioning forest carbon fluxes with overstory and understory eddy-
786   covariance measurements: A synthesis based on FLUXNET data. Agricultural and Forest
787   Meteorology, 144(1-2): 14-31.
788 Moncrieff, J., Clement, R., Finnigan, J. and Meyers, T., 2005. Averaging, detrending, and
789   filtering of eddy covariance time series. In: X. Lee, W. Massman and B. Law (Editors),
790   Handbook of Micrometeorology. Atmospheric and Oceanographic Sciences Library.
791   Springer Netherlands, pp. 7-31.

792 Morgenstern, K. et al., 2004. Sensitivity and uncertainty of the carbon balance of a Pacific
793   Northwest Douglas-fir forest during an El Nino La Nina cycle. Agricultural and Forest
794   Meteorology, 123(3-4): 201-219.
795 Novick, K., Brantley, S., Miniat, C.F., Walker, J. and Vose, J.M., 2014. Inferring the
796   contribution of advection to total ecosystem scalar fluxes over a tall forest in complex
797   terrain. Agricultural and Forest Meteorology, 185: 1-13.
798 Pan, Y.D. et al., 2011. A large and persistent carbon sink in the world's forests. Science,
799   333(6045): 988-993.
800 Papale, D. et al., 2006. Towards a standardized processing of net ecosystem exchange measured
801   with eddy covariance technique: Algorithms and uncertainty estimation. Biogeosciences,
802   3(4): 571-583.
803 Rannik, U. et al., 2002. Fluxes of carbon dioxide and water vapour over Scots pine forest and
804   clearing. Agricultural and Forest Meteorology, 111(3): 187-202.
805 Reich, P.B. et al., 2003. The evolution of plant functional variation: Traits, spectra, and
806   strategies. Int J Plant Sci, 164(3): S143-S164.
807 Richardson, A. and O'Keefe, J., 2009. Phenological differences between understory and
808   overstory. In: A. Noormets (Editor), Phenology of Ecosystem Processes. Springer New
809   York, pp. 87-117.
810 Ruehr, N.K., Knohl, A. and Buchmann, N., 2010. Environmental variables controlling soil
811   respiration on diurnal, seasonal and annual time-scales in a mixed mountain forest in
812   Switzerland. Biogeochemistry, 98(1-3): 153-170.
813 Siqueira, M.B. et al., 2006. Multiscale model intercomparisons of CO_2 and H_2O exchange rates
814   in a maturing southeastern US pine forest. Global change biology, 12(7): 1189-1207.
815 Sparling, J.H., 1967. Assimilation rates of some woodland herbs in Ontario. Bot Gaz, 128(3-4):
816   160-&.
817 Speckman, H.N. et al., 2015. Forest ecosystem respiration estimated from eddy covariance and
818   chamber measurements under high turbulence and substantial tree mortality from bark
819   beetles. Global change biology, 21(2): 708-721.
820 Staebler, R.M. and Fitzjarrald, D.R., 2004. Observing subcanopy CO2 advection. Agric. For.
821   Meteorol., 122(3-4): 139-156.
822 Teuling, A.J. et al., 2010. Contrasting response of European forest and grassland energy
823   exchange to heatwaves. Nat Geosci, 3(10): 722-727.
824 Thomas, C. et al., 2008. Estimating daytime subcanopy respiration from conditional sampling
825   methods applied to multi-scalar high frequency turbulence time series. agricultural and
826   forest meteorology, 148(8): 1210-1229.
827 Thomas, C.K., Martin, J.G., Law, B.E. and Davis, K., 2013. Toward biologically meaningful net
828   carbon exchange estimates for tall, dense canopies: Multi-level eddy covariance
829   observations and canopy coupling regimes in a mature Douglas-fir forest in Oregon.
830   Agricultural and Forest Meteorology, 173: 14-27.
831 Tota, J. et al., 2008. Amazon rain forest subcanopy flow and the carbon budget: Santarem LBA-
832   ECO site. J Geophys Res-Biogeo, 113: 10.1029/2007JG000597.
833 van Gorsel, E., Harman, I.N., Finnigan, J.J. and Leuning, R., 2011. Decoupling of air flow above
834   and in plant canopies and gravity waves affect micrometeorological estimates of net
835   scalar exchange. Agricultural and Forest Meteorology, 151(7): 927-933.

836   Vickers, D., Irvine, J., Martin, J.G. and Law, B.E., 2012. Nocturnal subcanopy flow regimes and
837   missing carbon dioxide. Agricultural and Forest Meteorology, 152: 101-108.
838   Vickers, D. and Mahrt, L., 1997. Quality control and flux sampling problems for tower and
839   aircraft data. J Atmos Ocean Tech, 14(3): 512-526.
840   Vickers, D. and Thomas, C.K., 2013. Some aspects of the turbulence kinetic energy and fluxes
841   above and beneath a tall open pine forest canopy. Agricultural and Forest Meteorology,
842   181: 143-151.
843   Webb, E.K., Pearman, G.I. and Leuning, R., 1980. Correction of flux measurements for density
844   effects due to heat and water-vapor transfer. Q J Roy Meteor Soc, 106(447): 85-100.
845   Wilczak, J., Oncley, S. and Stage, S., 2001. Sonic anemometer tilt correction algorithms.
846   Boundary-Layer Meteorology, 99(1): 127-150.
847   Wingate, L. et al., 2015. Interpreting canopy development and physiology using a European
848   phenology camera network at flux sites. Biogeosciences, 12(20): 5995-6015.
849   Wolf, S. et al., 2013. Contrasting response of grassland versus forest carbon and water fluxes to
850   spring drought in Switzerland. Environmental Research Letters, 8(3).
851   Wolf, S. et al., 2016. Warm spring reduced carbon cycle impact of the 2012 US summer drought.
852   Proceedings of the National Academy of Sciences of the United States of America,
853   113(21): 5880-5885.
854
855
856
857
858
859
860
861
862
863
864
865
866
867
868
869
870
871
872
873
874
875
876
877
878
879
880
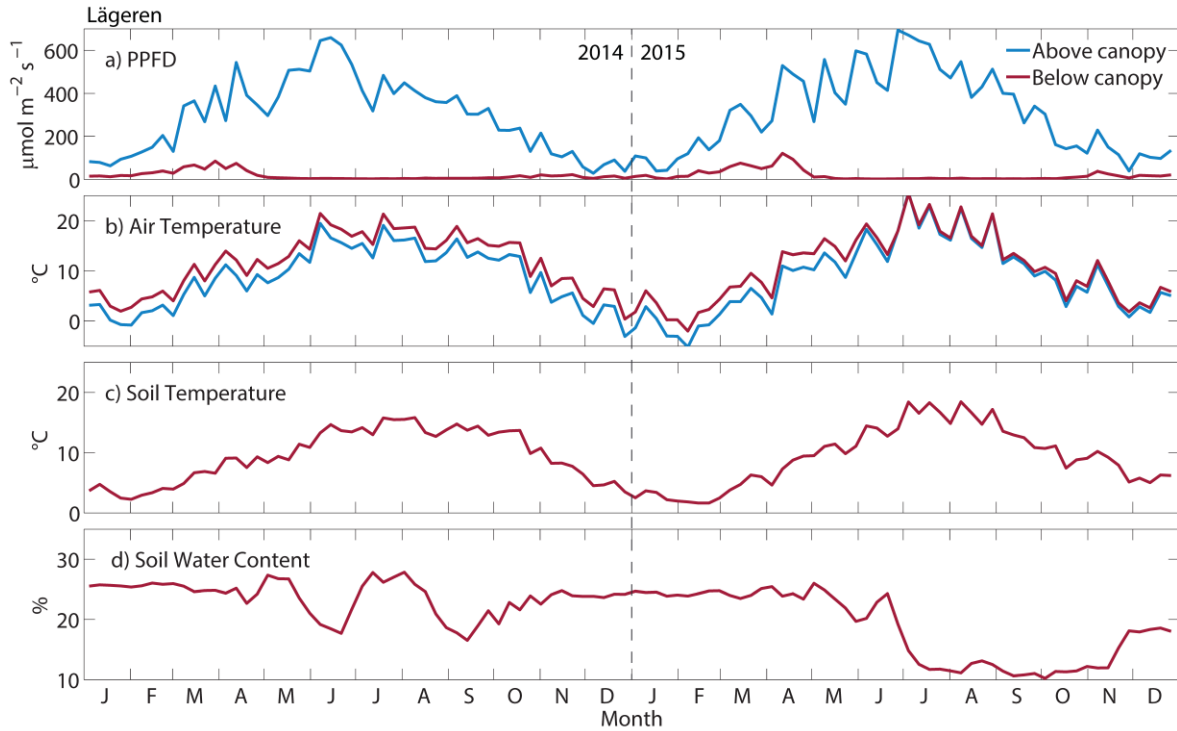
Figures

884 **Figure 1:** Climatic variables for a) photosynthetic photon flux density (PPFD), b) air temperature, c) soil
885 temperature and d) soil water content at Lägeren in 2014 and 2015. The blue lines represent above-canopy
886 measurements, while the red lines represent below-canopy measurements. Air temperature above canopy was
887 measured at 54 m height and below canopy at 2 m height. Soil temperature was measured at 5 cm depth and the soil
888 water content at 10 cm depth. All lines are 5-day averages.
889
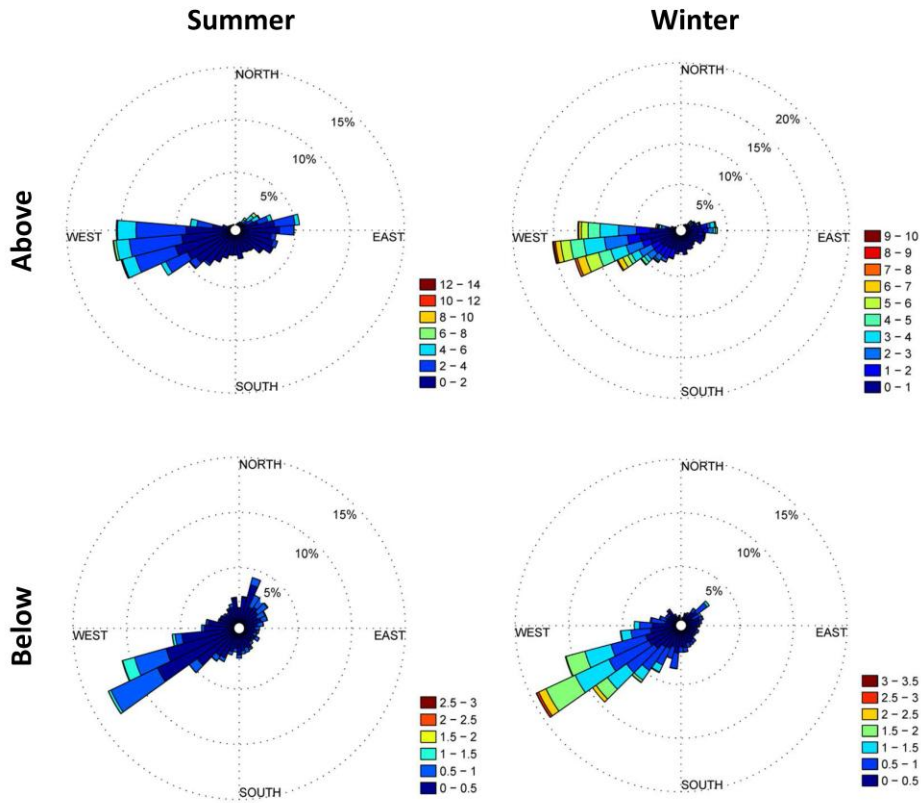
Figure 2: Distribution of wind directions (%) and respective wind speeds (m s^{-1}) in 2014 at Lägeren for above (54 m) and below (2 m) canopy in summer and winter. Seasons are defined based on the meteorological definition for summer (JJA) and winter (DJF). A similar wind distribution was found in 2015. Please note the different scaling between seasons.

900
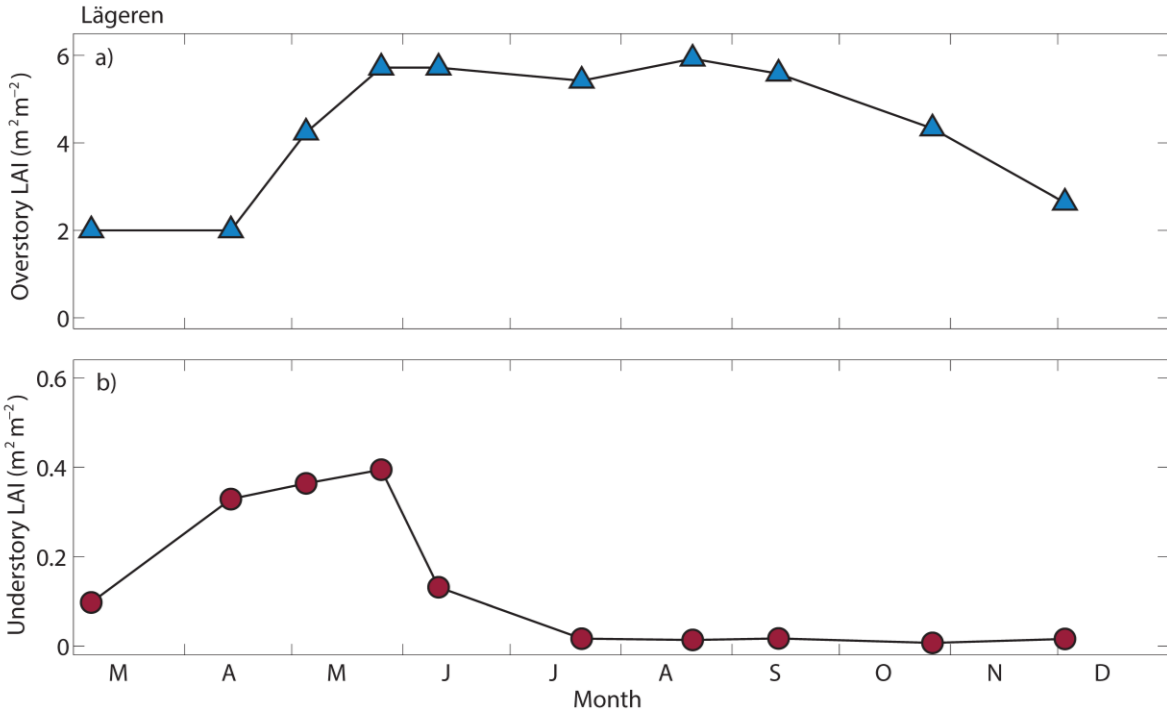
Figure 3: Overstory and understory LAI during the 2015 growing season at Lägeren. The blue triangles in a) represent the average of two transects of ten LAI measurements and the red circles in b) represent LAI estimated following Ernst (1979) from the biomass measurements. Please note the factor of 10 difference in y-axis scaling between panel a) and b).

905
906

907
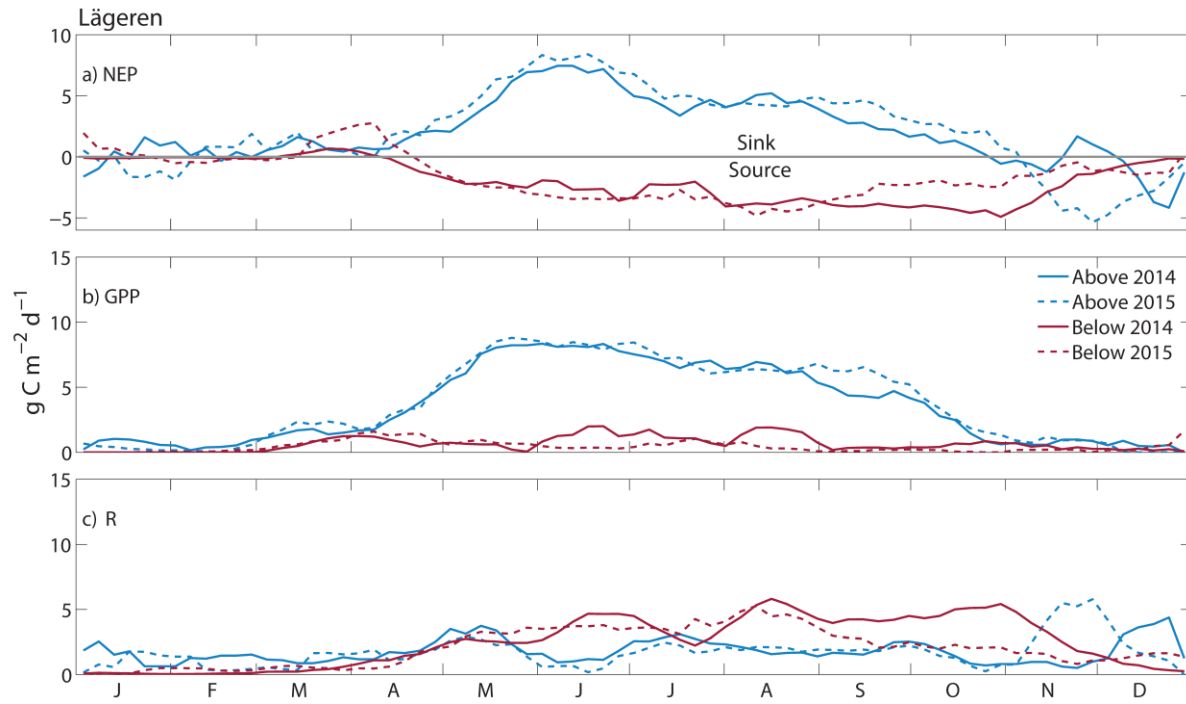
Figure 4: Measured net ecosystem production (NEP, panel a), gross primary production (GPP, panel b) and
respiration (*R*, panel c) above and below the canopy (without decoupling correction) at Lägeren in 2014 and 2015.
All lines are 5-day averages.
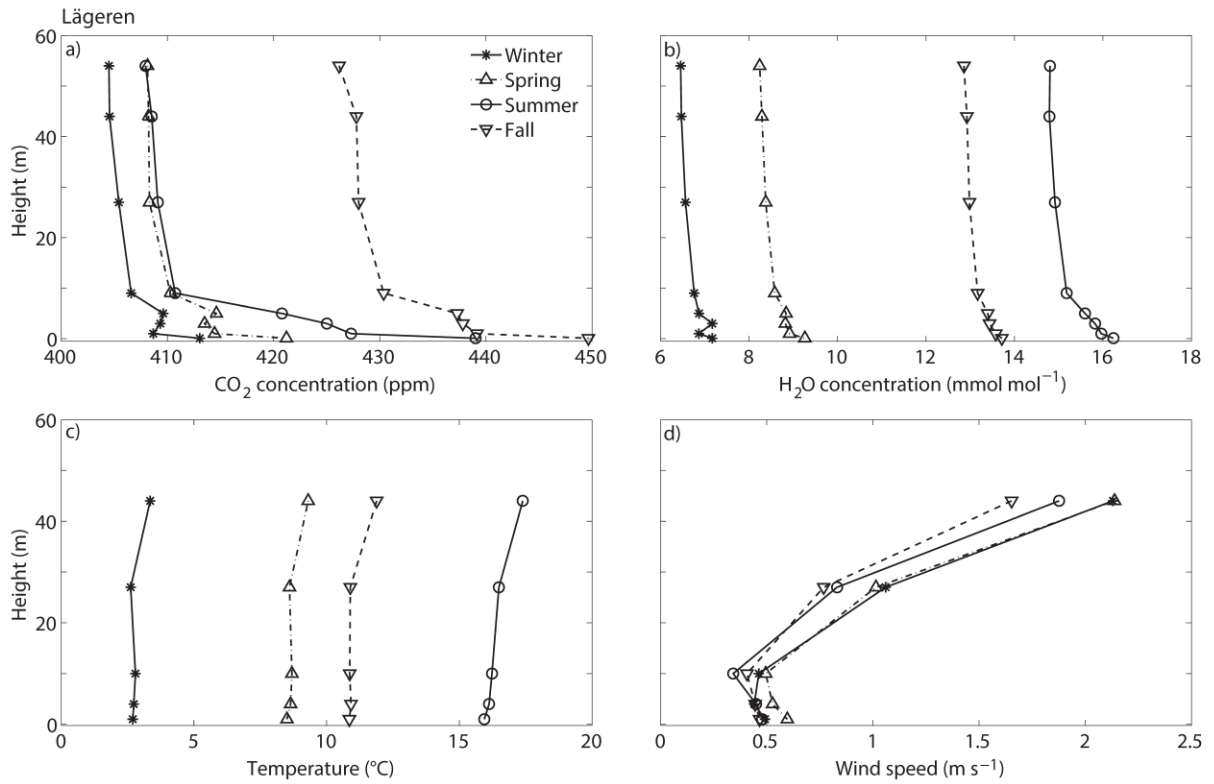
Figure 5: Seasonal profiles of mean a) CO_2 concentration, b) H_2O vapor concentration, c) temperature and d) wind speed within the canopy at Lägeren in 2014. Seasons are defined based on the meteorological definition for winter (DJF), spring (MAM), summer (JJA) and fall (SON). The average tree canopy height is 30 m, with the average tree canopy crown extending from 25 to 35 m. See supplementary Figure S 2 for daytime and nighttime profiles.

925
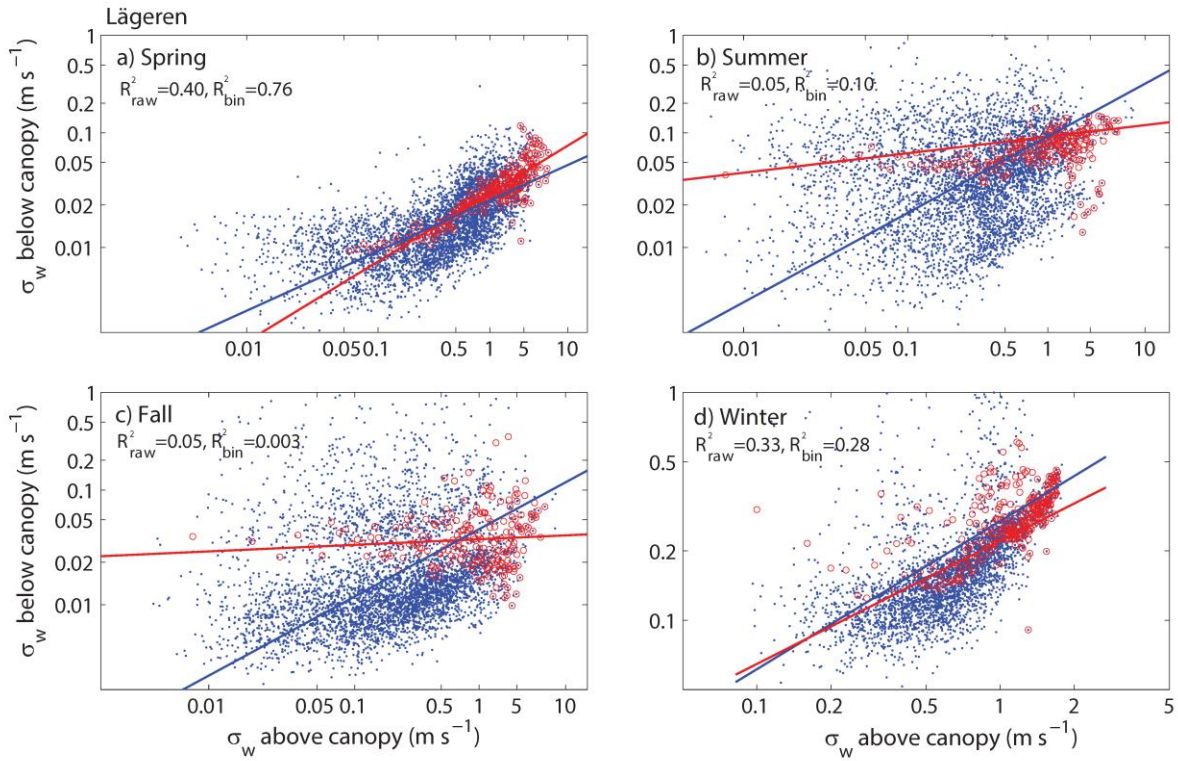
Figure 6: Relationships between standard deviations in vertical velocity (σ_w) below and above canopy for a)

spring, b) summer, c) fall and d) winter in 2014. Seasons are defined based on the meteorological definition for

winter (DJF), spring (MAM), summer (JJA) and fall (SON). The blue dots represent the half-hourly measurements

over the 5 days and the red circles are binned by 0.05 m s^{-1}.
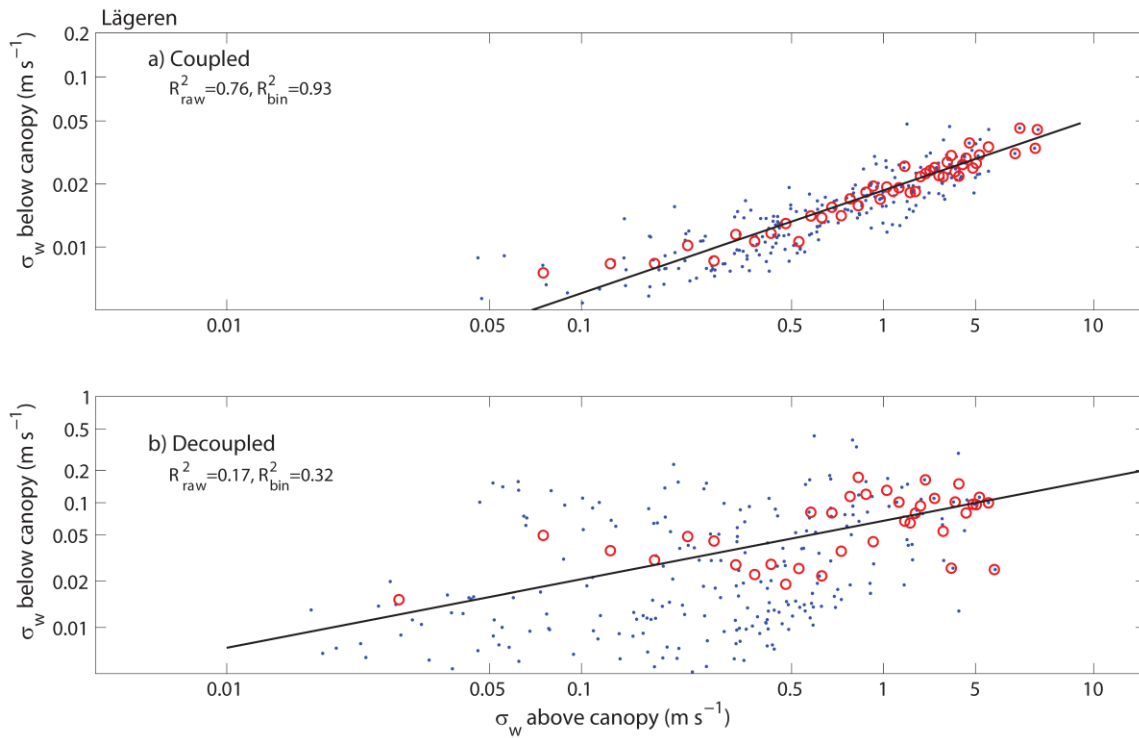
Figure 7: Standard deviation in vertical wind velocity (σ_w) for below and above canopy for the 5-day moving window showing an example for the a) coupled condition (May 10 to 15 2014) and b) decoupled condition (June 9 to 14 2014). The blue dots represent the half-hourly measurements over the five days and the red circles are binned by 0.05 m s^{-1}.

41
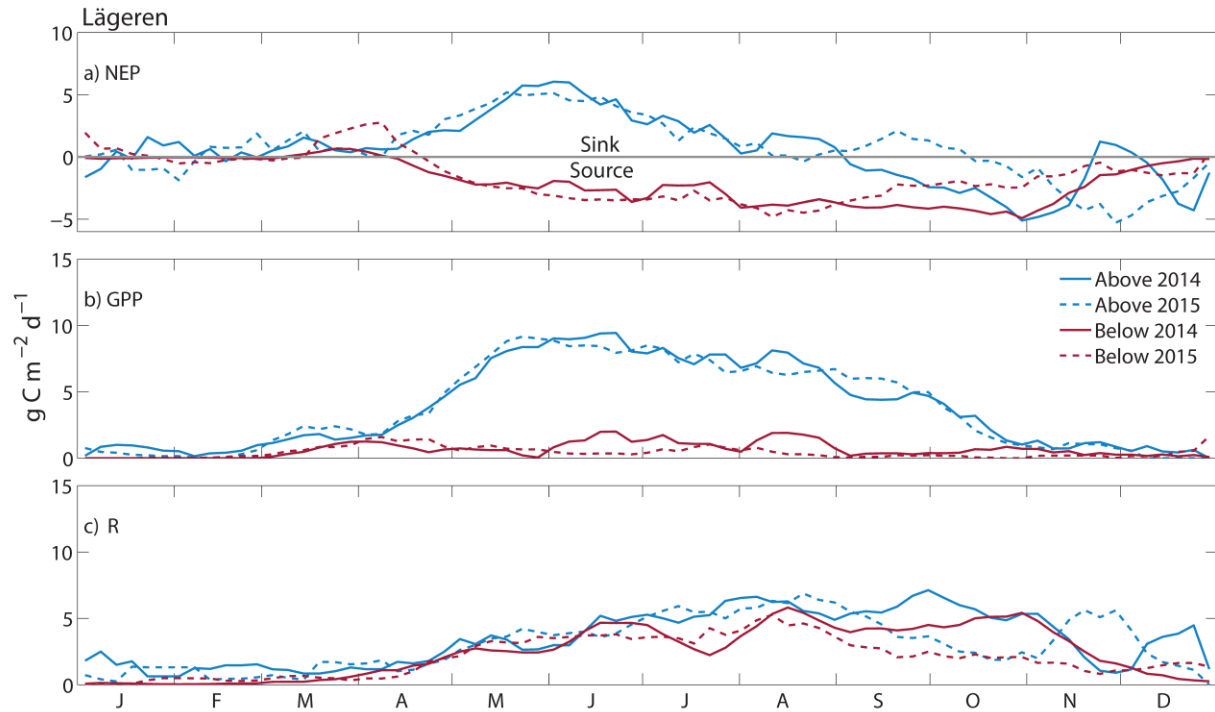
Figure 8: Net ecosystem production (NEP, panel a), gross primary production (GPP, panel b) and respiration (*R*, panel c) above the canopy after the decoupling correction and below the canopy in 2014 and 2015. All lines are 5-day averages.
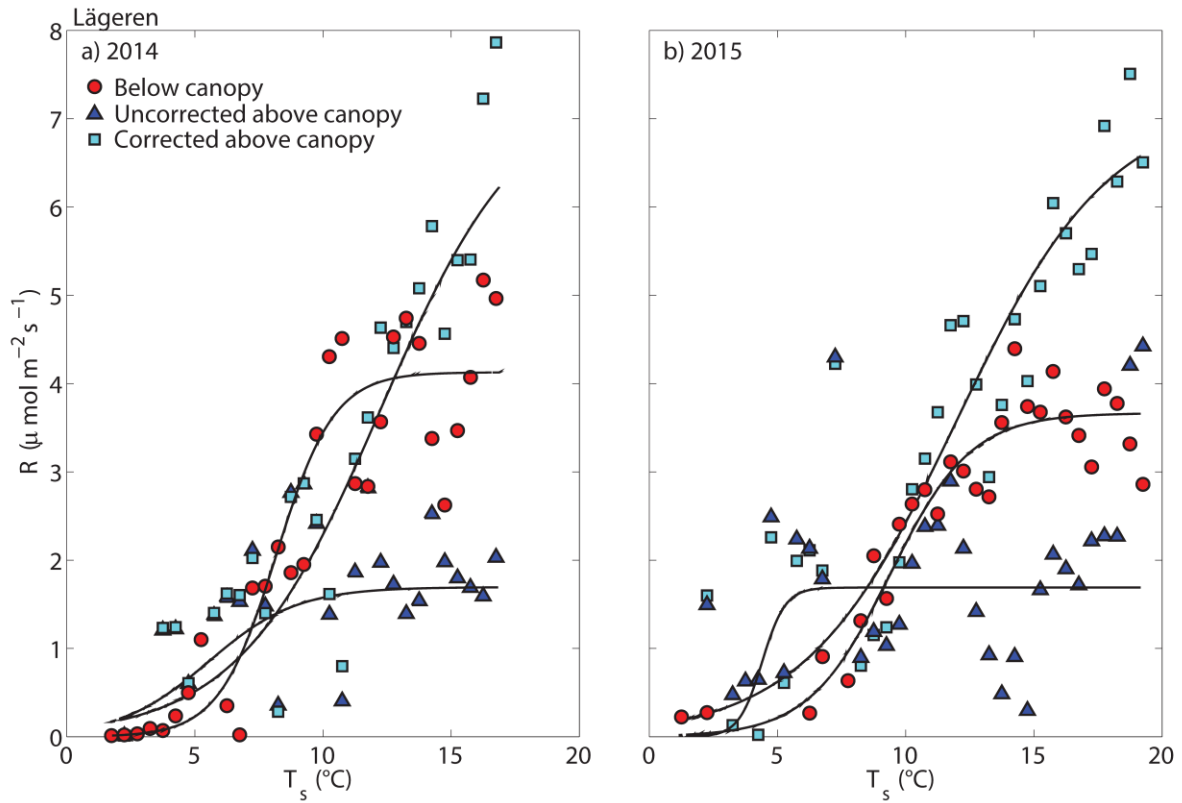
Figure 9: Respiration (R) versus soil temperature (T_s) at 5 cm depth at Lägeren in a) 2014 and b) 2015 for below canopy (red circles), uncorrected above canopy (blue triangles) and corrected above canopy (light blue squares). The lines are logistic equation (Eq. 1) fits to the measured half-hourly data (not binned) and the parameters are shown in Table 2. T_s values are binned in 0.5°C increments.
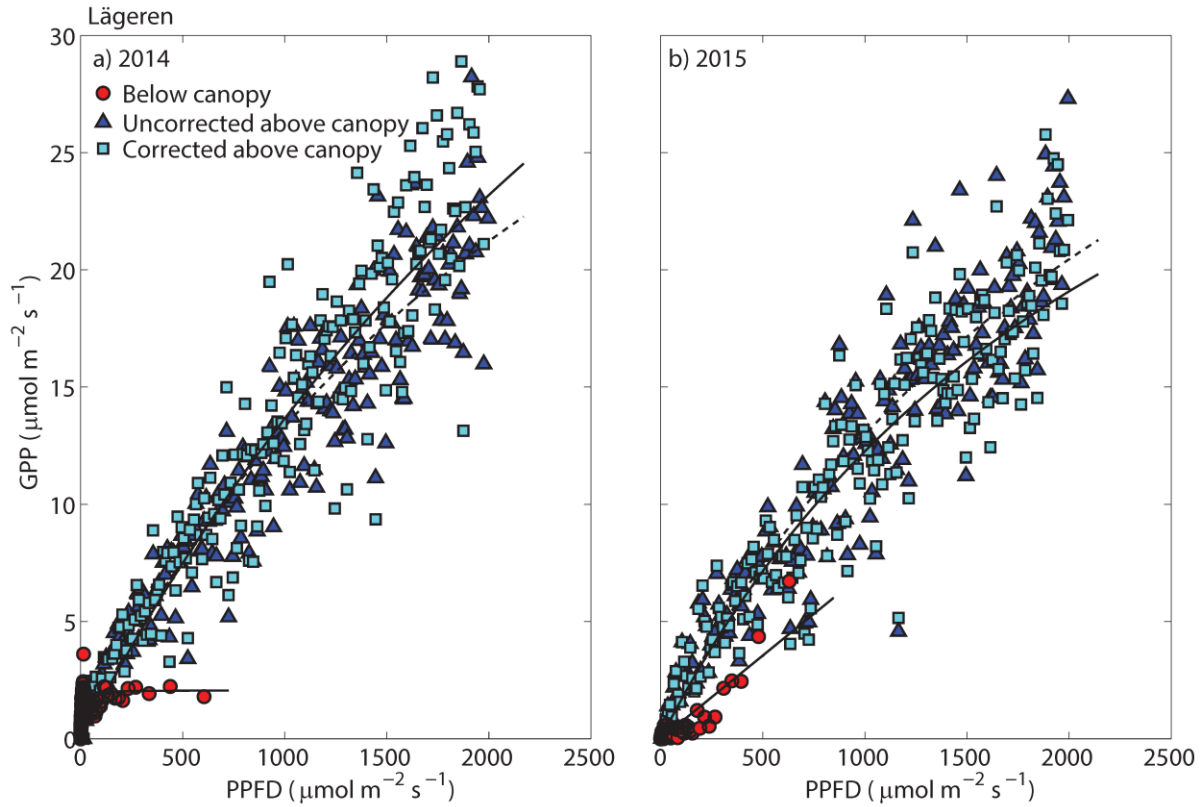
Figure 10: Gross primary production (GPP) as a function of downwelling photosynthetic photon flux density (PPFD) at Lägeren in a) 2014 and b) 2015 for below canopy (red circles), uncorrected above canopy (blue triangles) and corrected above canopy (light blue squares). The lines represent rectangular hyperbolic fits (Eq. 2) to the measured half-hourly data (not binned) and the values of the parameters are given in Table 3. PPFD values are binned in 50 µmol increments except for below-canopy values which are binned in increments of 50 values. The dashed line shows the uncorrected above canopy fit.

971

Figure 11: Average annual ecosystem CO_2 fluxes at the Lägeren site as measured above canopy uncorrected, with decoupling correction, and from biomass inventories combined with models. The bars in the shaded area represent the global averages for temperate deciduous forest from the synthesis study from Luyssaert et al. (2007). The bars represent the mean and error bars the standard deviation. Bars in green represent gross primary production (GPP), in brown represent respiration (R), and in red represent net ecosystem production (NEP).

972
973
974
975
976
977
978
979
980
981
982
983
984
985
986
987
988
989
990
991
992
993
994
995
996

Tables

Table 1: Annual sums (g C m^{-2} yr^{-1}) for below canopy, uncorrected above canopy, above canopy with decoupling correction, and below canopy percent contribution for net ecosystem production (NEP), gross primary production (GPP) and respiration (R) in 2014 and 2015.

Year	Flux (g C m^{-2} yr^{-1})	Below canopy uncorrected	Above canopy uncorrected	Above canopy corrected	Below canopy contribution with correction (%)
2014	NEP	-711	748	331	-
	GPP	187	1247	1325	14%
	R	898	499	995	90%
2015	NEP	-582	768	323	-
	GPP	57	1257	1269	4%
	R	639	489	945	68%
Mean ± SE	NEP	-647 ± 65	758 ± 10	327 ± 4	-
	GPP	122 ± 65	1252 ± 5	1297 ± 28	9%
	R	769 ± 130	494 ± 5	970 ± 25	79%

Table 2: Parameters for the logistic fits (Eq. 1) between respiration (R) and soil temperature (T_s) at Lägeren for below canopy, uncorrected above canopy and corrected above canopy fluxes. The logistic equation was fitted to the measured data in 2014 and in 2015.

		r_1 (µmol m^{-2} s^{-1})	r_2 (°C^{-1})	r_3 (°C)	R^2
2014	Below canopy	4.13	0.89	8.18	0.64
	Uncorrected above canopy	1.70	0.58	5.52	0.46
	Corrected above canopy	7.40	0.36	12.24	0.81
2015	Below canopy	3.67	0.63	9.34	0.48
	Uncorrected above canopy	1.69	2.20	4.40	0.21
	Corrected above canopy	7.16	0.34	12.00	0.74

Table 3: Parameters for the rectangular hyperbolic relationships between gross primary production (GPP) and photosynthetic photon flux density (PPFD) (Eq. 2) at Lägeren for below canopy, uncorrected above canopy and corrected above canopy fluxes. The equation was fitted to the measured data in 2014 and in 2015.

|		α (mol C mol^{-1} photons)	P_x (µmol m^{-2} s^{-1})	R^2
2014	Below canopy	0.45	2.07	0.46
	Uncorrected above canopy	0.02	52.40	0.82
	Corrected above canopy	0.02	76.82	0.78
2015	Below canopy	0.05	7.66	0.98
	Uncorrected above canopy	0.02	48.57	0.99
	Corrected above canopy	0.02	42.97	0.87

Table 4: Annual above-canopy net ecosystem production (NEP) at Lägeren in 2014 and 2015 without any correction, with a u_* threshold of 0.3 m s^{-1}, after accounting for 36% advection (according to Etzold et al. 2010), with the decoupling correction as well as NEP based on biomass inventories and modeled respiration.

NEP (g C m^{-2} yr^{-1})	No correction No u_*	No correction With u_*	No correction -36% advection	With correction No u_*	Biomass inventories and models
2014	748	501	477	331	321-341
2015	768	570	491	323	321-341
Mean ± SE	758 ± 10	536 ± 35	484 ± 7	327 ± 4	331 ± 10

1016   **Supplementary Material**
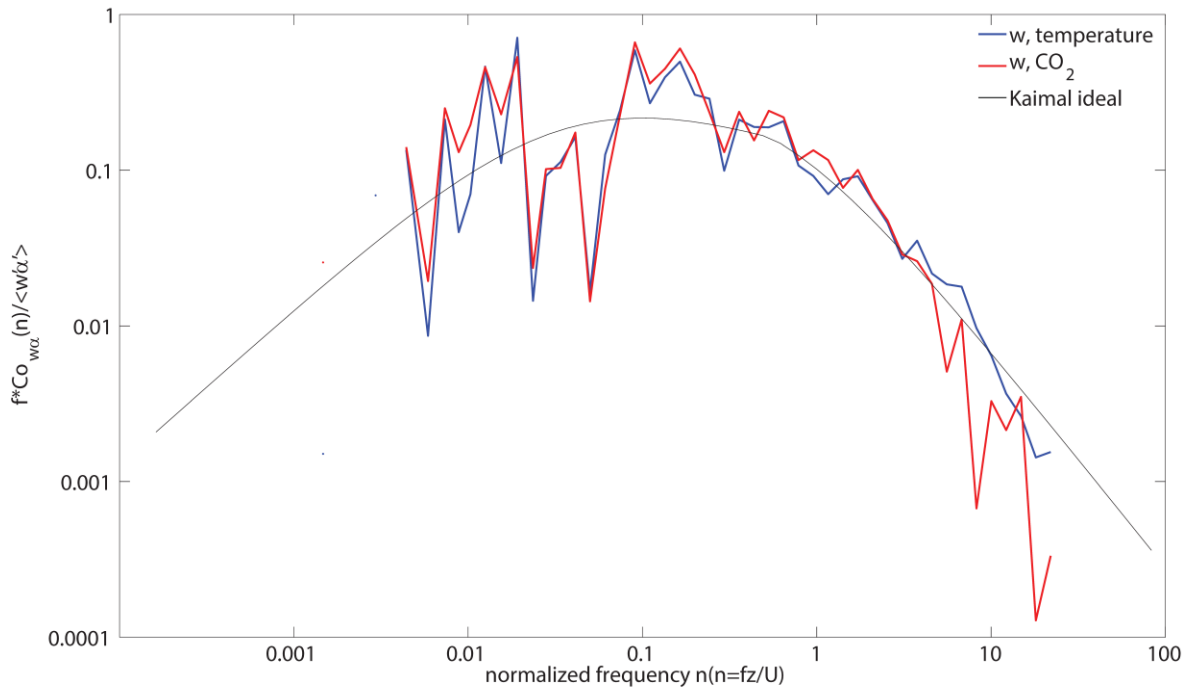
1017
1018   **Figure S 1:** Typical below-canopy cospectra of vertical wind and temperature (blue line) and vertical wind and CO_2
1019   (red line). The black line represents the ideal cospectra from Kaimal et al. (1972).
1020
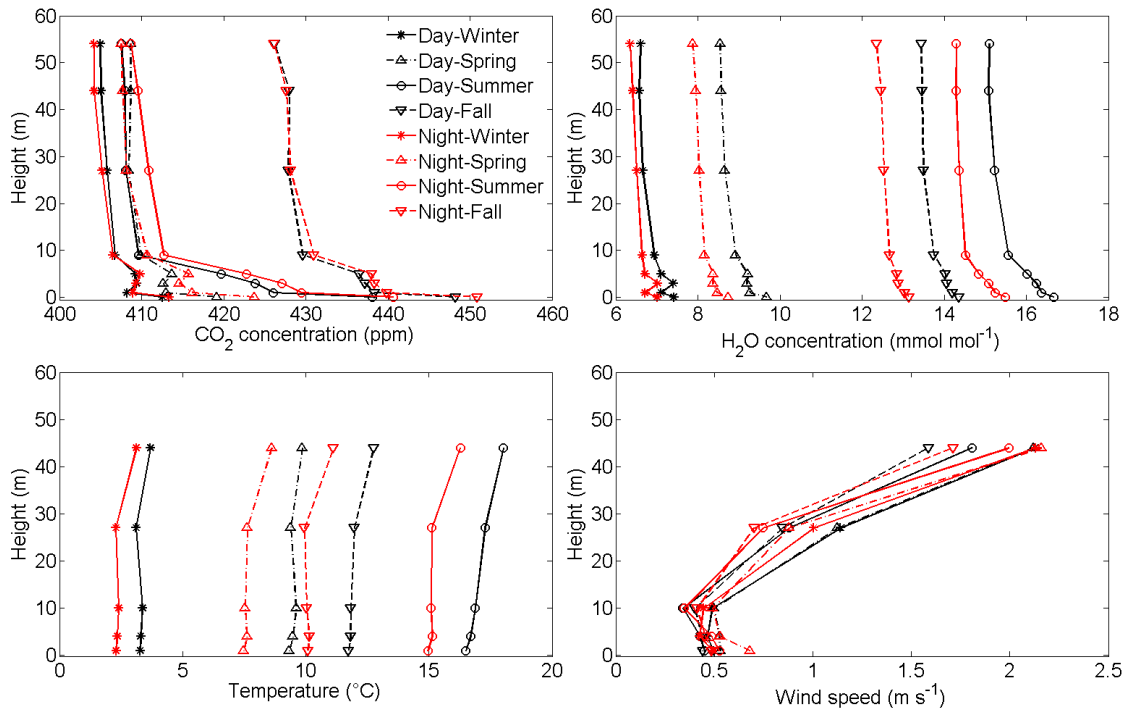
1021

1022 **Figure S 2:** Seasonal profiles of mean daytime (black) and nighttime (red) a) CO_2 concentration, b) H_2O vapor
1023 concentration, c) temperature and d) wind speed within the canopy at Lägeren in 2014. Seasons are defined based on
1024 the meteorological definition for winter (DJF), spring (MAM), summer (JJA) and fall (SON). The average tree
1025 canopy height is 30 m, with the average tree canopy crown extending from 25 to 35 m.

1026
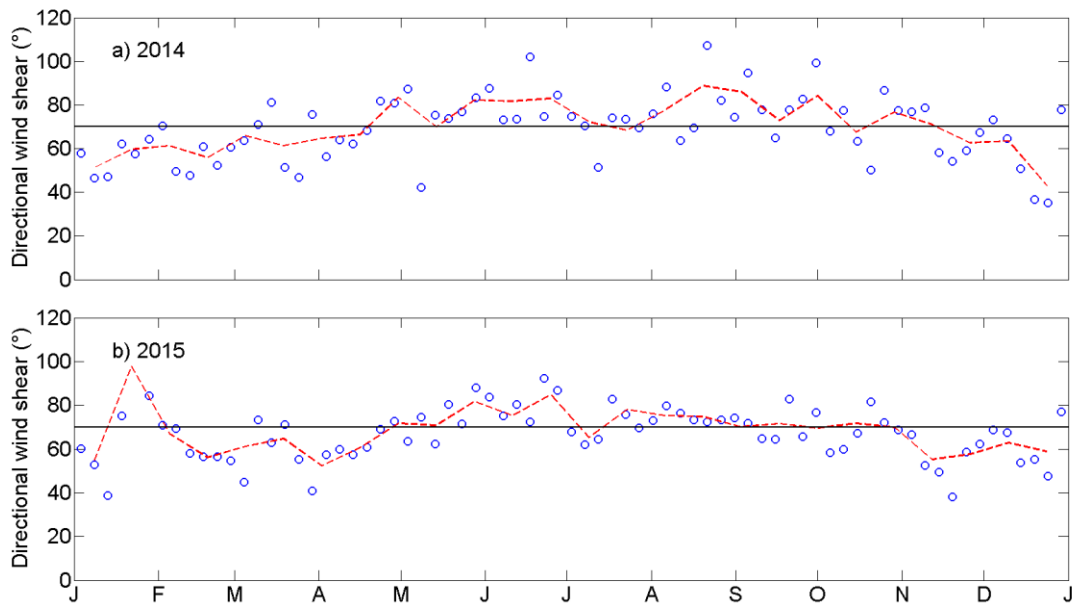
Figure S 3: Directional wind shear at the Lägeren site in a) 2014 and b) 2015. The blue circles represent 5-day averages and the red lines represent 14-day averages. The black line at 70° shows that wind shear during decoupled periods tend to be greater than 70 degrees, although this is not consistent.
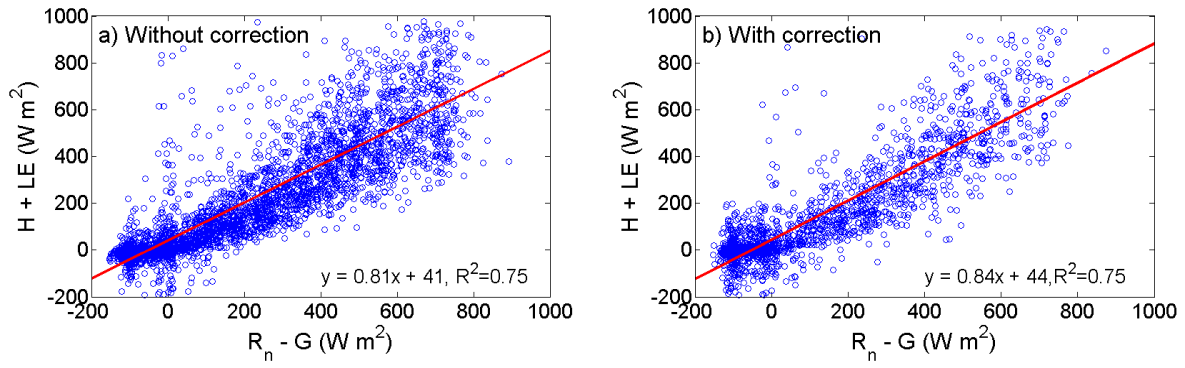
49
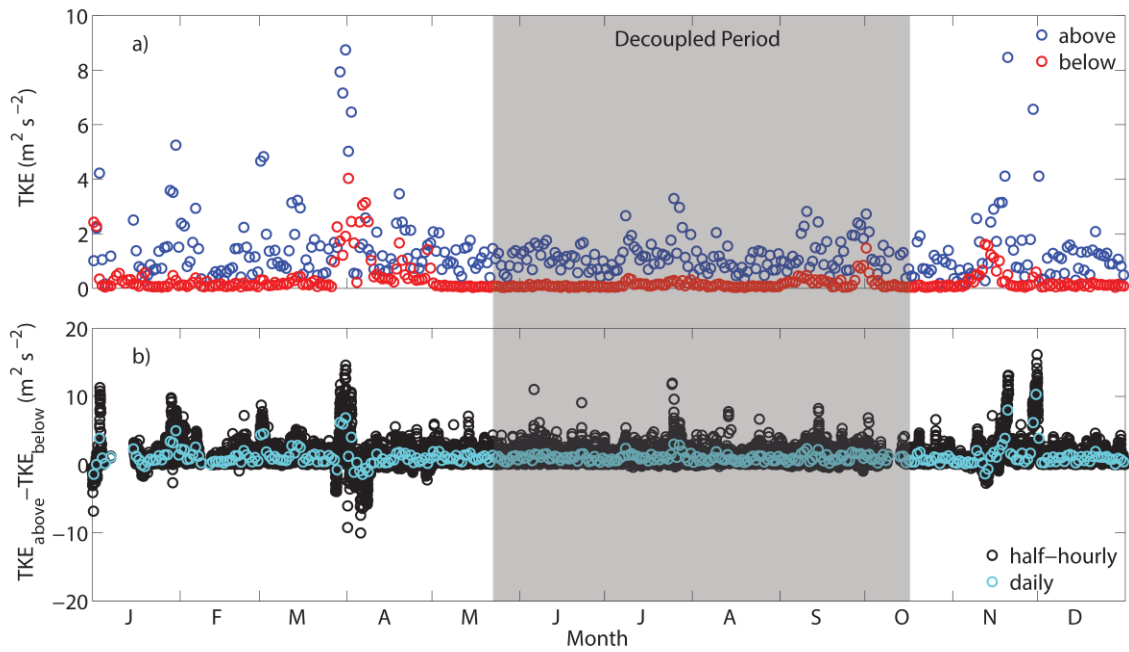
Figure S 4: Turbulent kinetic energy (TKE) a) above (blue) and below (red) the canopy, and b) difference in TKE above and below canopy in 2015. The circles in panel a) represent daily averages. The black circles in panel b) represent the half-hourly data while the cyan circles represent daily averages. The shaded area represents the decoupled period.
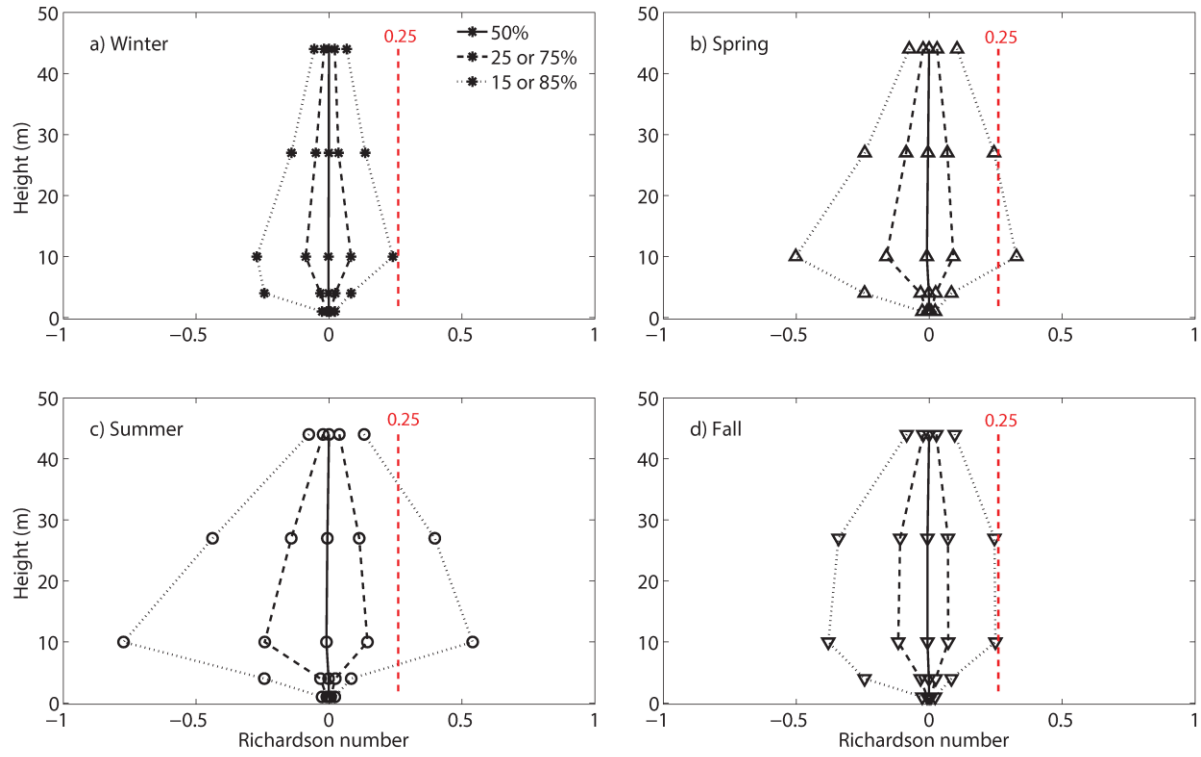
1038

Figure S 5: Richardson numbers in a) winter, b) spring, c) summer, and d) fall. The red line at 0.25 shows the critical Richardson number. The filled line shows the mark for 50% of the data, the dashed line for 25% and 75% of the data, and the dotted line for 15 and 85% of the data.

1039
1040
1041
1042

a) Without correction

$y = 0.81x + 41, R^2=0.75$

b) With correction

$y = 0.84x + 44, R^2=0.75$

Figure S 6: Energy balance closure a) without the decoupling correction and b) with the decoupling correction during the decoupled period in 2014.
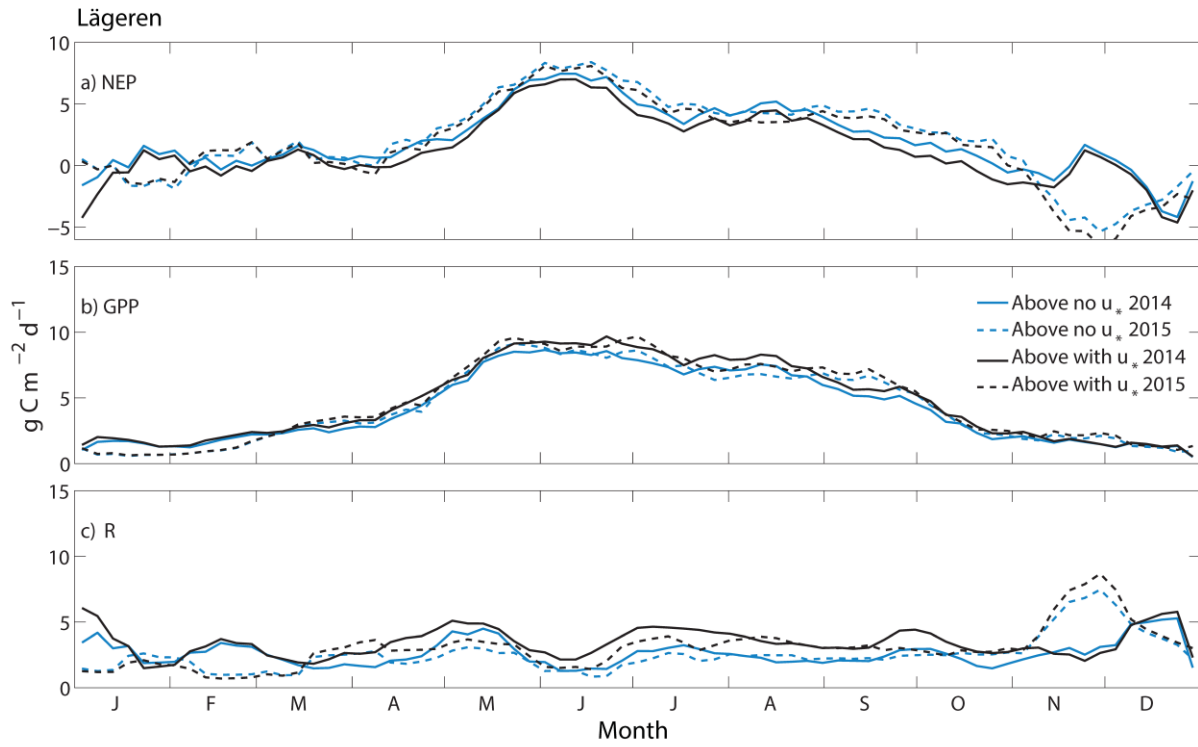
Figure S 7: Net ecosystem production (NEP), gross primary production (GPP) and respiration (R) above the canopy without (blue lines) and with (black lines) the u_* filtering in 2014 and 2015. All lines are 5-day averages.